SANDIA REPORT

SAND97-2391 • UC-704
Unlimited Release
Printed October 1997

PbO-Free Glasses for Low Temperature Packaging

Richard K. Brow, Denise N. Bencoe, David R. Tallant, Larry Kovacic

Prepared by
Sandia National Laboratories
Albuquerque, New Mexico 87185 and Livermore, California 94550

Sandia is a multiprogram laboratory operated by Sandia Corporation, a Lockheed Martin Company, for the United States Department of Energy under Contract DE-AC04-94AL85000.

Sandia National Laboratories

Issued by Sandia National Laboratories, operated for the United States Department of Energy by Sandia Corporation.

Available to DOE and DOE contractors from
Office of Scientific and Technical Information
PO Box 62
Oak Ridge, TN 37831

Prices available from (615) 576-8401, FTS 626-8401

Available to the public from
National Technical Information Service
US Department of Commerce
5285 Port Royal Rd
Springfield, VA 22161

NTIS price codes
Printed copy: A08
Microfiche copy: A01

SAND97-2391
Unlimited Release
Printed September 1997

Distribution
Category UC-704

PbO-Free Glasses for Low Temperature Packaging

Richard K. Brow and Denise N. Bencoe
Materials Joining Department

David R. Tallant
Surface And Sensor-Controlled Processes Department

Larry Kovacic
Ceramic & Glass Processing Department

Sandia National Laboratories
P. O. Box 5800
Albuquerque, NM 87185-1349

Abstract

Zinc polyphosphate glasses were examined as potential candidates for low temperature sealing applications. Glass-formation and properties were determined for the ZnO-P_2O_5, ZnO-B_2O_3-P_2O_5, and ZnO-SnO-P_2O_5 systems, and information about the short-range structures of these glasses was obtained by Raman and solid state nuclear magnetic resonance spectroscopies. In general, the most durable polyphosphate glasses have structures based on relatively short pyrophosphate chain lengths (i.e., 2 P-tetrahedra). Modified phosphate compositions are given, including compositions used to seal float glass substrates at temperatures as low as 500°C.

Acknowledgments

The authors thank R. L. Simpson of the Surface & Sensor-Controlled Processes Department for collecting the Raman spectra; S. T. Myers (formerly of Sandia) and G. L. Turner (Spectral Data Services, Champaign, IL) for collecting the solid state nuclear magnetic resonance spectra. The authors also thank Jill Glass (Materials Joining Department) for her careful review of this document.

Contents

Figures

Tables

PbO-Free Materials for Low Temperature Packaging

Introduction

PbO-based solder glasses have an unusual combination of low sealing temperature and relatively low coefficient of thermal expansion (CTE), making them the inorganic sealing material of choice for a variety of electronic and optoelectronic packaging applications (see, *e.g.*, Frieser 1975 and references therein). PbO, however, is a toxic material and regulatory concerns are the primary reason for replacing PbO-based materials. For example, in New York, flat panel displays which are scrapped during manufacturing must be treated as hazardous waste because of the PbO-solder glass used to join front and back plates. A second drawback to PbO-solder glasses is that they typically must be sealed in oxidizing conditions to prevent reduction to Pb-metal. This precludes their use in a variety of electronics applications that require low temperature packaging of air or oxygen sensitive components.

Glasses based on the $ZnO-P_2O_5$ system are potential substitutes for PbO-based solder glasses in many sealing applications. Alkali zinc pyrophosphate compositions (*viz*., based on the $(P_2O_7)^{4-}$ anion) have glass transition temperatures below 400°C while retaining excellent chemical durabilities (Beall and Quinn 1990; Quinn *et al*. 1992). Glasses from the $SnO-ZnO-P_2O_5$ system possess even lower transition temperatures and lower coefficients of thermal expansion (CTE), while retaining chemical durabilities comparable to PbO-solder glasses (Aitken *et al.* 1993; Francis and Morena 1994). When mixed with the proper low expansion filler, these Sn-Zn-phosphate glasses form low temperature sealing materials that have expansion matches to a variety of potential substrates (Morena 1996).

In the present study we have examined the structures and properties of glasses from several zinc phosphate-based systems, including alkali-modified compositions and those based on the SnO (and SnF_2)-$ZnO-P_2O_5$ system. We report Raman and nuclear magnetic resonance (NMR) spectra that reveal compositionally dependent changes in the molecular bonding of these systems that can be related to changes in glass properties. We also report the results of sealing experiments, using both conventional furnaces and a CO_2-laser, of modified Zn-phosphate glasses designed to have a CTE match to float glass.

II. Glass Properties and Structures

II-1 Zinc Phosphate Glasses

This section summarizes our study of the glasses in the $xZnO\ (1-x)P_2O_5$ system. For further details, see Brow *et al.* (1995).

Glasses were prepared from reagent grade ZnO and $NH_4H_2PO_4$, with nominal ZnO contents between 50 and 71 mole%. Although glasses can be prepared with significantly lower ZnO contents (Kordes 1941; Knatak and Hummel 1958), such ultraphosphate compositions would contain significant concentrations of structural water (Abe 1983) unless prepared under special conditions and so were not examined in the present study. Raw materials were thoroughly mixed, then melted in Pt crucibles in air for one hour near 1000°C; some attack of the Pt could be detected. Most glasses were poured onto steel plates, annealed for thirty minutes near T_g, then stored in a desiccator prior to analyses. Melts with ZnO contents >65 mole% were quenched between two steel plates to prevent crystallization. A melt containing 73 mole% ZnO crystallized to β-$Zn_3(PO_4)_2$ immediately upon quenching.

Most of the glasses were transparent with some small bubbles. The P_2O_5-content of each sample was analyzed by inductively coupled plasma atomic emission spectrometry (ICP-AES) and the ZnO-content was determined by difference. Each sample was analyzed in duplicate and the results of those analyses are given in Table 2-1; the estimated uncertainty is ±5% relative. Except for some slight P_2O_5 volatility from several melts, there is little change in composition during glass formation. For simplicity, a glass will be identified by its 'as-batched' composition; the analyzed composition, however, will be used when discussing the quantitative relationships between glass structure and composition.

The refractive index of each sample was measured using the Becke line technique. The accuracy of this measurement for most samples is the difference in **n** for our comparative fluids (±0.002); however, significant dispersion in some samples produced uncertainties approaching ±0.004. Densities (ρ) were measured in Freon using the Archimedes method. At least two samples of each composition were measured and the average value is reported. The estimated uncertainty is ±0.005 g/cm^3. Molar volumes were then calculated using molar weights based on the analyzed glass composition ($MV=MW/\rho$). Glass transition temperatures (T_g) were determined by differential thermal analyses using heating rates of 5°C/min; these temperatures are reproducible to ±3°C. Several of these properties are also summarized in Table 2-1.

Molecular bonding arrangements were characterized by magic angle spinning nuclear magnetic resonance (MAS NMR) and Raman spectroscopies (R. K. Brow *et al*. 1995). Most ^{31}P MAS NMR spectra were collected at 147.1 MHz (H_0=8.45 T), using 11 μsec pulses and 10 sec recycle times with spinning speeds of 7-9 kHz. Several MAS spectra were also collected at 162.0 MHz, using 5 μsec pulses and relaxation delays as long as 1200 sec with spinning speeds of 8 kHz. All ^{31}P NMR chemical shifts are expressed in ppm relative to an 85% H_3PO_4 solution; isotropic peak positions are reproducible to about ±0.4 ppm. In general, chemical shifts were independent of experimental parameters. Relative site concentrations were determined by decomposing each spectrum, including spinning side bands, into a series of gaussian peaks, then summing the respective areas of these peaks. A number of samples were run in duplicate and we found that the respective site concentrations were reproducible to ±10%.

Table 2-1: Composition and properties of binary ZnO-P_2O_5 glasses.

Batched ZnO (mole%)	Analyzed ZnO (mole%)	density (g/cm^3)	Refr. Index	T_g (°C)
50.0	51.7	2.875	1.521	451
52.5	52.4	2.964	1.533	415
55.0	55.5	3.056	1.545	425
57.5	57.6	3.182	1.563	417
60.0	59.5	3.294	1.576	416
62.5	62.0	3.366	1.586	416
65.0	65.6	3.523	1.604	446
66.7	66.1	3.611	1.614	432
69.0	69.5	3.781	1.632	465
71.0	71.1	3.875	1.641	467

Glass samples were also characterized by Raman spectroscopy using a computer controlled scanning double monochromator equipped with holographic gratings and a cooled photomultiplier tube (RCA C31034). The 514.5 nm line of an argon ion laser provided the excitation. The monochromator was operated at a resolution of 6 cm^{-1}.

The molar volume (MV, determined from the density measurements) and refractive index (n) for each zinc polyphosphate glass examined in this study are shown in Figure 2-1 (closed circles) and compared with values reported by Kordes (1941) for similar glasses (open circles). Molar volume and refractive index both change monotonically with increasing ZnO content; there are no obvious breaks in either series that might reveal a significant structural change within the compositional range studied. The molar volumes of crystalline $Zn(PO_3)_2$ (Averbuch-Pouchot *et al*. 1983), α-$Zn_2P_2O_7$ (Robertson and Calvo 1970), and α-$Zn_3(PO_4)_2$ (Calvo 1965), calculated from their respective reported densities, are also plotted in Figure 2-1 (closed diamonds). The molar volumes for the 50 mole% ZnO and 67 mole% ZnO glasses, higher than the respective molar volumes of crystalline $Zn(PO_3)_2$ and α-$Zn_2P_2O_7$, imply that the glasses have a significantly more open molecular structure, most likely because of a lower average Zn coordination number (Brow et al. 1995).

Figure 2-2 shows the ^{31}P MAS NMR spectra from a number of the binary glasses. Isotropic chemical shifts are labeled with Q^i values (where 'i' represents the number of bridging oxygens per phosphate tetrahedron); the remaining peaks are spinning sidebands that arise from the anisotropies of the Q^2 and Q^1 sites. These peak assignments are consistent with those made in other ^{31}P NMR studies of polyphosphate glasses (Villa *et al*. 1987; Prabhakar *et al*. 1987; Brow *et al*. 1990).

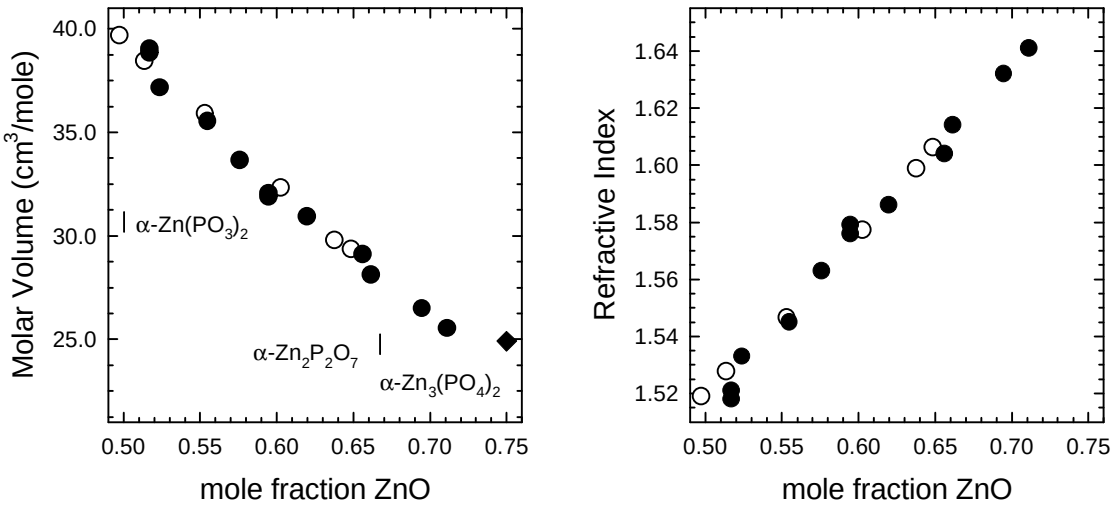

Figure 2-1: Properties of binary zinc phosphate glasses. Molar volumes (left) and refractive indices (right) from glasses prepared for this study (closed symbols) and those reported by Kordes (1941). The closed diamonds represent the molar volumes of crystalline zinc phosphates.

The spectrum from the metaphosphate (0.50 ZnO) glass is dominated by an isotropic peak near -32 ppm, representing the Q^2 tetrahedra that are the bases for metaphosphate chains. The intensity of this peak (and its associated sideband pattern), decreases relative to the intensity of a second isotropic peak (and sideband pattern), centered near -12 ppm, as the ZnO-content increases. These new features are due to Q^1 sites that either terminate chains or are found in isolated pyrophosphate dimers. A third isotropic peak, centered near +5 ppm, is present in the spectra from glasses with ZnO contents in excess of about 60 mole%, and becomes the dominant feature in the spectrum from the 71 mole% ZnO glass. This latter chemical shift is comparable to those reported for crystalline orthophosphates (Turner *et al*. 1986b) and the lack of an extensive sideband pattern is consistent with our assignment of this peak to more symmetric Q^0 P tetrahedra.

Figure 2-3 shows an expanded spectrum from the pyrophosphate glass (67 mole% ZnO) decomposed into Gaussian contributions from each of the three different isotropic peaks. Site concentrations were calculated from the respective areas of each isotropic peak and its associated sidebands. Table 2-2 lists the isotropic chemical shifts and estimated site concentrations, the latter determined for each glass from the relative peak areas of the decomposed ^{31}P MAS NMR spectra.

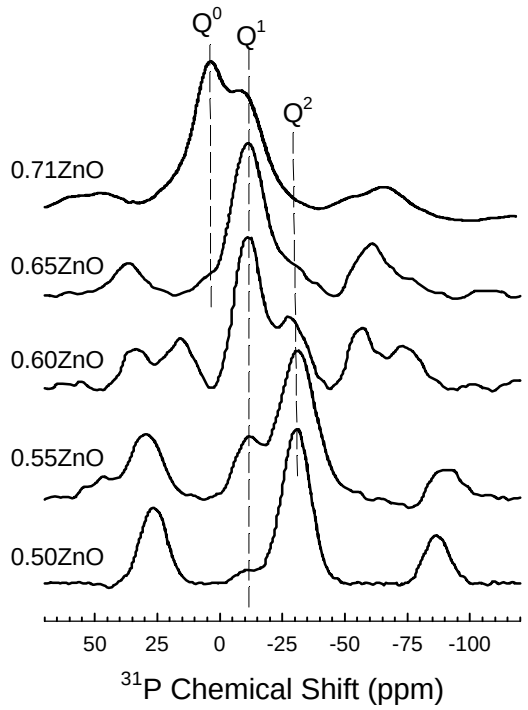

Figure 2-2: **^{31}P MAS NMR (147.1 MHz) spectra for several xZnO•(1-x)P_2O_5 glasses**. Isotropic peaks are labeled using the 'Q^i' notation and the remaining peaks are spinning sidebands.

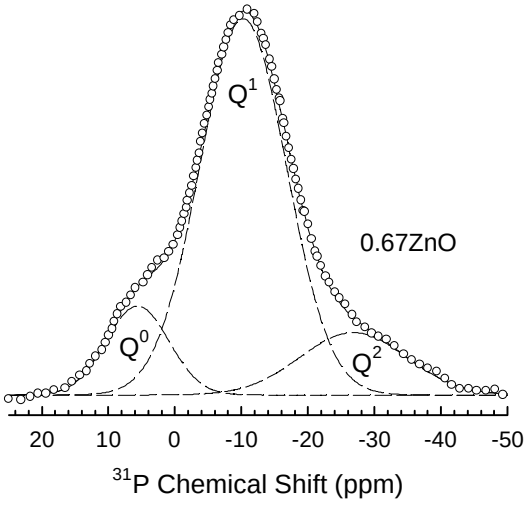

Figure 2-3: **Decomposed ^{31}P MAS NMR spectrum for the 0.67ZnO•0.33P_2O_5 glass.** The spectrum, collected at 147.1 MHz, shows the disproportionation of the Q^1 (-10.7 ppm) sites into Q^0 (+5.6 ppm) and Q^2 (-28.6 ppm) sites. The open circles represent the 'as-collected' spectrum, the dashed lines are the three Gaussian components, and the solid line is the sum of the three components.

Table 2-2: ^{31}P NMR chemical shifts (ppm relative to 85% H_3PO_4) and relative peak and spinning sideband areas.

mole% ZnO	Mag. field	Q^2 Area	Q^2 ppm	Q^1 Area	Q^1 ppm	Q^0 Area	Q^0 ppm
51.7	147.1 MHz	0.96	-31.4	0.04	-12.8	0.00	---
51.7	162.0 MHz	0.96	-31.1	0.04	-12.8	0.00	---
55.5	147.1 MHz	0.80	-31.7	0.20	-13.1	0.00	---
59.5	147.1 MHz	0.40	-30.4	0.60	-11.8	0.00	---
59.5	162.0 MHz	0.54	-30.6	0.46	-12.7	0.00	---
62.0	147.1 MHz	0.36	-30.4	0.60	-13.7	0.03	+5.1
65.6	147.1 MHz	0.19	-29.7	0.74	-12.3	0.07	+5.6
66.1	147.1 MHz	0.13	-28.6	0.75	-10.7	0.13	+5.6
66.1	162.0 MHz	0.22	-29.1	0.66	-12.0	0.12	+3.6
69.5	162.0 MHz	~0.02	~-30	0.64	-11.1	0.34	+4.0
71.1	147.1 MHz	0.00	---	0.62	-10.2	0.36	+4.8
71.1	162.0 MHz	0.00	---	0.53	-10.7	0.47	+4.0

Figure 2-4 shows partial Raman spectra from six zinc polyphosphate glasses ranging in composition from $50ZnO\bullet 50P_2O_5$ to $71ZnO\bullet 29P_2O_5$. The spectra are comparable to those reported by Quinn *et al*. (1992) for similar zinc polyphosphate compositions. The evolution of the Raman spectra implies progressive depolymerization of the phosphate networks with increasing zinc concentration. Band assignments are given in Table 2-3 (see Brow *et al*. 1995, for details).

When ZnO is added to $Zn(PO_3)_2$, metaphosphate chains are terminated by pyrophosphate structures according to the pseudo-reaction:

$$Q^2 + ZnO \rightarrow 2Q^1. \qquad (2\text{-}1)$$

This 'chemical order' structural model predicts that reaction (2-1) will continue up to the pyrophosphate composition ($2ZnO\bullet P_2O_5$), at which the stoichiometry requires that only Q^1 dimers be present, as is the case for crystalline α- and β-$Zn_2P_2O_7$ (Robertson and Calvo 1970; Calvo 1965).

The systematic increase in the ratio of non-bridging to bridging oxygens (characterized quantitatively in section II-2 by x-ray photoelectron spectroscopy) associated with the Q^1 tetrahedra contributes to the monotonic increase in the refractive index shown in Figure 2-1 and an increase in the concentration of Q^1 sites is in qualitative agreement with the ^{31}P NMR and Raman spectral trends noted above. We can use the simple chemical order structural model described by reaction (2-1) to predict the quantitative relationships between the composition of $xZnO\ (1\text{-}x)P_2O_5$ glasses (where 'x' is the mole fraction of ZnO) and the relative fraction of Q^1 and Q^2 sites in the metaphosphate-to-pyrophosphate series (Brow *et al*. 1990):

$$f_{Q1} = (2x\text{-}1)/(1\text{-}x), \qquad (2\text{-}2a)$$
$$f_{Q2} = (2\text{-}3x)/(1\text{-}x). \qquad (2\text{-}2b)$$

For glasses with $0.667 \leq x \leq 0.75$, only Q^1 and Q^0 sites are expected from the chemical order model at the following relative concentrations:

$$f_{Q^0} = (3x-2)/(1-x), \quad (2\text{-}2c)$$
$$f_{Q^1} = (3-4x)/(1-x). \quad (2\text{-}2d)$$

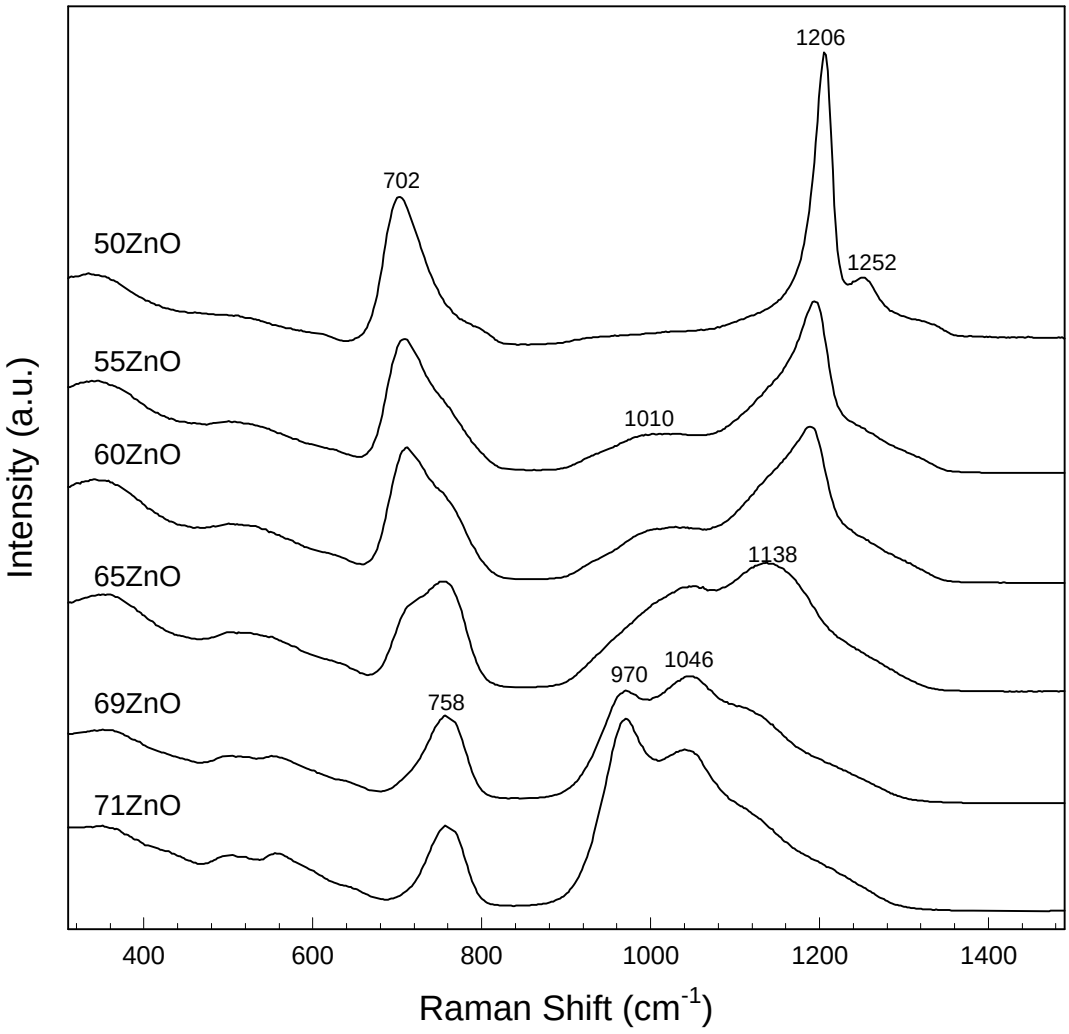

Figure 2-4: Raman spectra for several of the $xZnO \bullet (1-x)P_2O_5$ glasses.

Figure 2-5 compares the predicted site populations (solid lines) based on this simple model with those determined by NMR (Table 2-2); good agreement exists up to x~0.625. For glasses with ZnO contents approaching the pyrophosphate composition, there are fewer Q^1 and more Q^2 sites

Table 2-3: Raman bands and proposed peak assignments for Zn phosphate glasses.

Frequency	Assignment
~350 cm^{-1}	Bend mode of phosphate polyhedra with zinc modifier
571 cm^{-1}	Bend mode related to zinc-phosphate network or ZnO_4
704 cm^{-1}	POP_{sym} stretch (bridging oxygen), Q^2 species
757 cm^{-1}	POP_{sym} stretch (bridging oxygen), Q^1 species
969 cm^{-1}	$(PO_4)_{sym}$ stretch (nonbridging oxygen), Q^0 species
1010 cm^{-1}	P-O stretch, Q^1 chain terminator
1048 cm^{-1}	$(PO_3)_{sym}$ stretch (nonbridging oxygen), Q^1 species
1138 cm^{-1}	P-O stretch, Q^1 chain terminator
1206 cm^{-1}	$(PO_2)_{sym}$ stretch (nonbridging oxygen), Q^2 species
1253 cm^{-1}	$(PO_2)_{asym}$ stretch (nonbridging oxygen), Q^2 species

than are predicted, and there are significant concentrations of Q^0 sites, which are not predicted to be present by the simple chemical ordering model until $x>0.667$. In addition, there are fewer Q^1 sites, and more Q^0 and Q^2 sites than predicted for glasses with $x\geq0.667$. The Raman spectra are in qualitative agreement with these observations. The spectrum from the Zn pyrophosphate glass (Figure 2-4), for example, has shoulders near 1200 cm^{-1} and near 970 cm^{-1} that are due to $P\text{-}O^-$ bonds on Q^2 and Q^0 tetrahedra, respectively, even though reaction (2-1) predicts that only Q^1 tetrahedra will exist at this composition.

The excess Q^2 and Q^0 sites in the glasses with ZnO contents that approach and exceed the pyrophosphate composition apparently result from the disproportionation of Q^1 species in the glass melts:

$$2Q^1 \leftrightarrow Q^2 + Q^0. \qquad (2\text{-}3)$$

If we assume that the activity coefficients for each Q^i species are equal and that reaction (2-3) can be treated as a true chemical reaction, then we can estimate an equilibrium constant (k_1) for the pyrophosphate disproportionation reaction from:

$$k_1 = [Q^2][Q^0]/[Q^1]^2. \qquad (2\text{-}4)$$

Such reactions form the bases for van Wazer's 'Reorganization Theory' for the distribution of structures in phosphate liquids (Van Wazer 1958). Using concentrations based on the NMR areas given in Table 2-2, we calculate an equilibrium constant for reaction (2-3) of 0.028 ± 0.018.

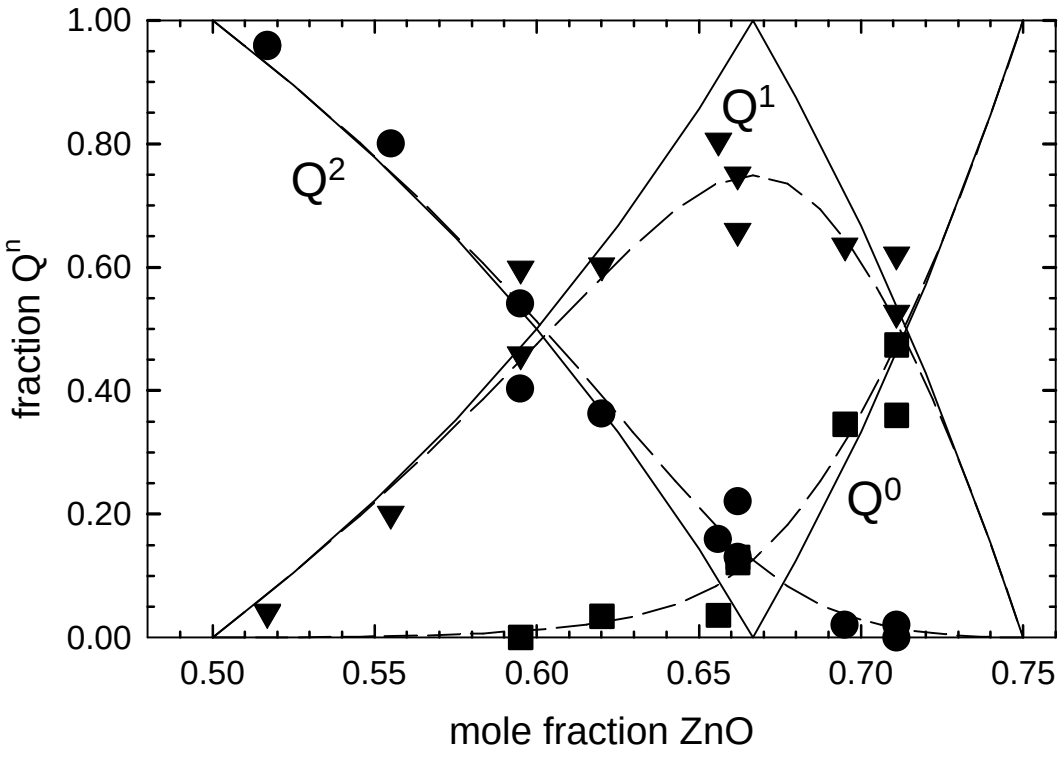

Figure 2-5: The effect of composition on the Q^i distributions determined by ^{31}P MAS NMR (closed symbols). The solid lines are the predicted relationships based on the simple chemical order model described by equations 2-2a-d. The dashed lines are the predicted relationships after accounting for Q^1 disproportionation.

This value is in good agreement with that (k_1=0.031) calculated from a chromatographic analysis of phosphate chain lengths in a Zn pyrophosphate glass quenched from a melt (Weyl and Marboe 1964), but is lower than that (k_1=0.09) calculated from a second chromatographic study of $60ZnO•40P_2O_5$ and $62.5ZnO•37.5P_2O_5$ glasses (Meadowcraft and Richardson 1965). (These differences are not particularly significant: the $Q^0/Q^1/Q^2$ fractions calculated from the chromatographic analyses of Meadowcraft and Richardson (1965) for the $62.5ZnO•37.5P_2O_5$ glass are 0.06/0.54/0.40, compared with 0.03/0.60/0.36 calculated for a similar glass in the present study.) The dashed lines in Figure 2-5 are the predicted site distributions after accounting for the disproportionation of Q^1 species, assuming k_1=0.028.

Figure 2-5 indicates that there is no comparable disproportionation of Q^2 sites; *viz.*, $2Q^2 \leftrightarrow Q^3 + Q^1$, k_2=0.0. This most likely is a consequence of the chemical instability of branched Q^3 structures in condensed phosphates (*viz.*, the 'Anti-Branching' rule (Van Wazer 1958) which leads to a very low equilibrium constant for Q^2 disproportionation and thus good agreement with the chemical order

model (reactions 2-2a and 2-2b) for the structure of glasses with compositions near the metaphosphate stoichiometry.

The disproportionation of Q^1 species in Zn-pyrophosphate melts has no discernible effect on the trends in the molar volume and refractive index data (Fig. 2-1); both of these properties should depend more on the relative bridging-to-nonbridging oxygen ratio which is insensitive to disproportionation. Other properties, however, may depend on the equilibrium conditions of reaction (2-3). Quinn *et al*. (1992) note that the Q^2 sites in a Zn-pyrophosphate glass are most susceptible to hydrolysis and that chemical durability improves when the composition is modified to suppress disproportionation and so reduce the Q^2 concentration. It seems reasonable that disproportionation also enhances glass formation by increasing the structural complexity of the pyrophosphate melt. It has been reported (Weyl and Marboe 1964) that metal pyrophosphates which disproportionate in the melt (Zn, Cd, and Bi) will form glasses when quenched, whereas those that do not disproportionate (K, Na, and Li) crystallize upon cooling.

In summary, the oxygen coordination environments of both phosphorus and zinc become more varied as ZnO is added to the zinc metaphosphate glass composition. It appears that tetrahedral zinc may be present in both the metaphosphate and pyrophosphate glasses, even though zinc does not occur in tetrahedral sites in the corresponding crystals. This coordination difference could be a factor contributing to the ease of glass formation from a pyrophosphate melt. In addition, the NMR data indicate that there is some disproportionation of the Q^1 groups to Q^0 and Q^2 species in the zinc pyrophosphate glass. This added structural complexity most likely also contributes to glass formation (i.e., stability against crystallization) at this composition.

II-2 Zinc Borophosphate Glasses

Zinc borophosphate glasses were prepared from mixtures of reagent grade ZnO, $NH_4H_2PO_4$, and H_3BO_3. The initial series consisted of compositions along the tie-line between Zn-pyrophosphate and B_2O_3 (Series I, Figure 2-6). These glasses were melted in platinum crucibles and some attack of the crucible was noted. All subsequent phosphate-containing compositions, including those along the zinc metaphosphate-B_2O_3 tie-line (series II), were prepared in high-purity (>99%) alumina crucibles. Each composition was melted in air for one hour at temperatures between 1000 and 1150ºC. Glasses were quenched on steel plates, annealed near T_g, then stored in desiccators prior to analyses.

The chemical compositions of a number of samples were determined by ICP-AES. In general, the nominal compositions were retained to ±5% relative. Glasses prepared in alumina crucibles contain <2mole% Al_2O_3 as an impurity.

Most of the glasses were clear with some small bubbles. Glasses in the pyrophosphate series with >15 mole% B_2O_3were phase-separated, forming a white, x-ray amorphous material. The Zn-metaphosphate glass containing 50 mole% B_2O_3 was also phase-separated.

Several properties were determined for the series I and II glasses. Glass transition temperatures (T_g) were determined by differential thermal analyses at a heating rate of 10°C/min; reported temperatures are reproducible to ±5°C. Thermal expansion coefficients were determined by dilatometry at 10°C/min and are reported as normalized length changes from room temperature to 300°C and with an estimated uncertainty of ±3 x 10^{-7}/°C. Densities were determined by the Archimedes method using Freon; at least two samples of each composition were characterized and the average is reported. Refractive indices were determined using the Becke line method using standard comparative liquids. Because of some dispersion in these samples, the estimated accuracy of the reported indices are ±0.004.

Figure 2-6 shows the compositions from the $ZnO \cdot B_2O_3 \cdot P_2O_5$ system studied here. Closed circles represent compositions which formed clear glasses and open circles represent phase-separated or crystallized compositions. The larger region of single-phase glass formation extends from the ZnO-P_2O_5 tie-line towards B_2O_3. A much smaller region extends from ~60$ZnO \cdot$40 B_2O_3 towards Zn-pyrophosphate. Melts from compositions between these two regions were phase-separated when cooled. For example, clear glasses could be formed in the xB_2O_3 $(1-x)Zn_2P_2O_7$ system for $0 \leq x \leq 0.15$ (series I) and in the yB_2O_3 $(1-y)Zn(PO_3)_2$ system for $0 \leq y \leq 0.40$ (series II). In both series, greater B_2O_3 contents lead to the formation of white, phase-separated samples. Glass formation in the B_2O_3-rich portion of Figure 2-6 was not determined.

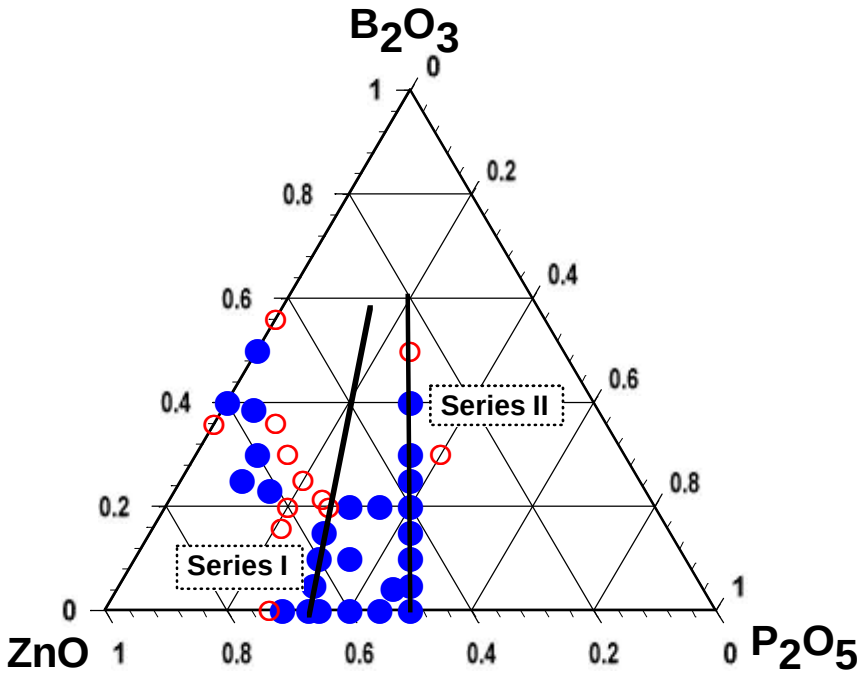

Figure 2-6: Zn-borophosphate compositions examined in this study. Closed circles are compositions which form clear glasses, open circles are those that do not. The lines represent compositions in series I (xB_2O_3 $(1-x)Zn_2P_2O_7$) and series II (yB_2O_3 $(1-y)Zn(PO_3)_2$).

Table 2-4: Selected properties of Zn-borophosphate glasses

B_2O_3	$Zn_2P_2O_7$	ρ (g/cm^3)	Refr. Index	T_g (°C)	T_x (°C)	$\alpha_{20\text{-}300}$ (10^{-7}/°C)
0.00	1.00	3.611	1.614	432	535	76
0.05	0.95	3.586	1.618	460	598	71
0.10	0.90	3.550	1.616	475	599	73
0.15	0.85	3.490	1.613	486	618	67
B_2O_3	$Zn(PO_3)_2$					
0.00	1.00	2.875	1.521	451		80
0.05	0.95	2.901	1.529	467		79
0.10	0.90	2.921	1.533	470		77
0.15	0.85	2.955	1.541	453		72
0.20	0.80	3.016	1.563	509		
0.25	0.75	2.996	1.555	510		73
0.30	0.70	3.009	1.560			71
0.35	0.65	3.004	1.560	510		70
0.40	0.60	2.977	1.564	519		69

Some of the properties of glasses from the B_2O_3/Zn-pyrophosphate and B_2O_3/Zn-metaphosphate series are listed in Table 2-4. In both series, the addition of B_2O_3 increases T_g. Density and refractive index increase in the metaphosphate series and decrease slightly in the pyrophosphate series.

Figure 2-7 shows the effect of B_2O_3-content on the molar volumes (MV=molar weight/density) of the two glass series. Molar volume decreases sharply when B_2O_3 is added to Zn-metaphosphate up to ~25-30 mole% B_2O_3, and then more slowly thereafter, whereas there is little change in molar volume in the much smaller B_2O_3/Zn-pyrophosphate glass forming system. The break in the series II MV data suggests that some change occurs in the short-range glass structure near 30 mole% B_2O_3.

Figure 2-8 shows the ^{11}B MAS NMR spectra collected from the series I (left) and series II (right) glasses. The spectra of low-B_2O_3 glasses in both series are dominated by a narrow, symmetric peak centered at about -3.8 ppm. Increasing the B_2O_3-content (>10 mole% in series I and >30 mole% in series II) results in the formation of a second narrow, symmetric peak, centered at -1.8 ppm, and the development of a broad, asymmetric feature that extends from about +20 to -15 ppm.

The two narrow symmetric peaks are due to tetrahedral B-sites, and the broad, asymmetric feature is due to trigonal B-sites (Bunker *et al*. 1991; Gan *et al*. 1994). Second-order quadrupolar interactions are responsible for the breadth and asymmetry of this latter feature (Turner *et al*. 1986a). No attempts were made to determine the quadrupolar coupling constants or asymmetry parameters for these sites.

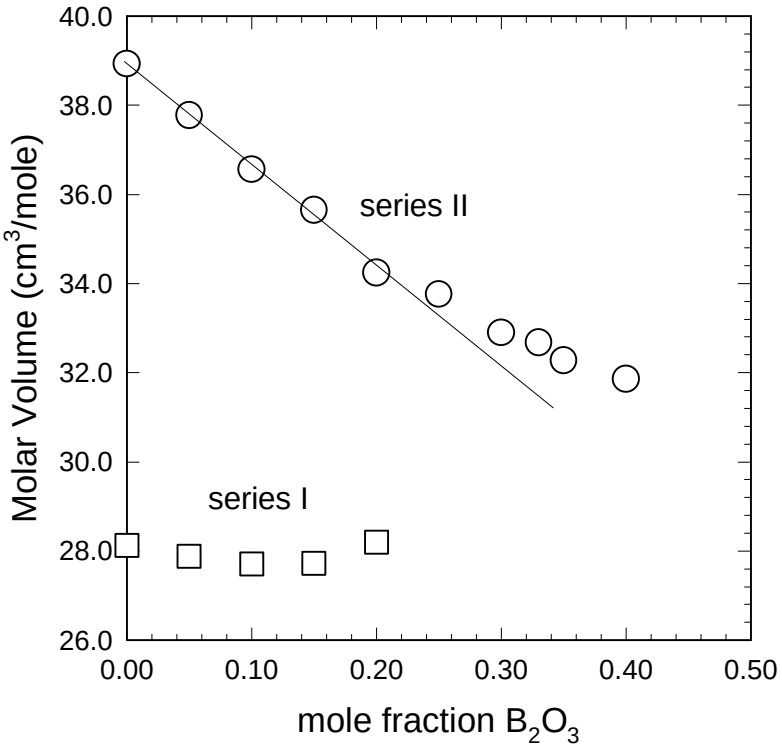

Figure 2-7: Molar volumes of Zn-borophosphate glasses. The line is drawn as a guide for the eye.

We have measured an ^{11}B MAS NMR chemical shift of -3.5 ppm for crystalline BPO_4, in good agreement with a value of -3.2 ppm reported in a previous study (Turner *et al*. 1986a) and so we assign the tetrahedral peak centered at -3.8 ppm in the Zn-borophosphate glasses to borons in a borophosphate environment; viz., $B(OP)_4$. We also examined a $50ZnO \cdot 50B_2O_3$ glass and recorded an ^{11}B NMR chemical shift for tetrahedral borons at +0.4 ppm. We expect that similar structures, viz., $B(OB)_4$, account for the deshielded tetrahedral peak, near -1.8 ppm, in the spectra from the higher B_2O_3 containing glasses. Table 2-5 summarizes the NMR peak assignments.

The maximum intensity of the asymmetric trigonal component to the ^{11}B MAS NMR spectra is centered near +9 ppm, in good agreement with previous MAS NMR studies of borate glasses (Turner *et al*. 1986a.; Bunker *et al*. 1990). The breadth of the B(III) feature is such that we have not attempted to deconvolve contributions from different trigonal sites; i.e., symmetric vs. asymmetric B(III)s. We have, however, estimated site concentrations by measuring the relative areas of the trigonal and tetrahedral spectral contributions. These relative concentrations are discussed below.

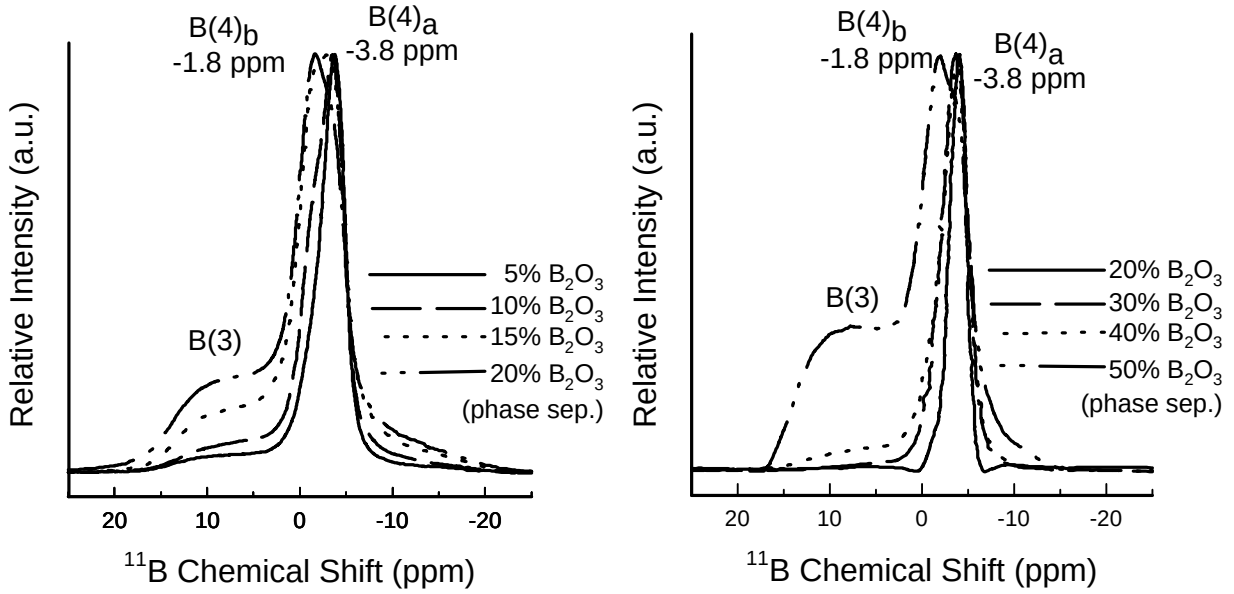

Figure 2-8: ^{11}B MAS NMR spectra collected from several of the series I (left) and series II (right) glasses. Spectra were collected at 116.6 MHz (H_0=8.45 T), using 3 μsec pulses and 1 sec recycle times with spinning speeds of 8-9 kHz.

Table 2-5: MAS NMR isotropic peak assignments for the indicated nuclei.

B$(OB)_4$	**B**$(OP)_4$	**B**(3)	**P**$(OB)_4$	**P**$(OP)_2(OZn)_2$	**P**$(OP)_1(OZn)_3$	**P**$(OZn)_4$
-1.8 ppm	-3.8 ppm	+9 ppm	-29 ppm	-31 ppm	-12 ppm	+5 ppm

^{31}P MAS NMR spectra (not shown) were collected from the two series. Table 2-5 lists our ^{31}P MAS NMR isotropic peak assignments.

Figure 2-9 shows the unpolarized Raman spectra collected from the series I glasses (left). The spectrum from the Zn-pyrophosphate base glass is dominated by a spectral envelope with distinct peaks at 1048 and 1124 cm^{-1}, a sharp peak at 757 cm^{-1}, and a broader peak centered at 351 cm^{-1}. Spectral assignments are consistent with the disproportionated mixed ortho-, pyro-, metaphosphate structures mentioned above and are discussed in Brow *et al*. (1995). The 1048 cm^{-1} and 1124 cm^{-1} bands are due to the symmetric stretches from Q^1 tetrahedra associated with pyrophosphates and terminal sites on polyphosphate chains. The 757 cm^{-1} band is due to the P-O-P stretching modes of pyrophosphate species, and the 351 cm^{-1} band is due to phosphate bending modes These assignments are summarized in Table 2-6.

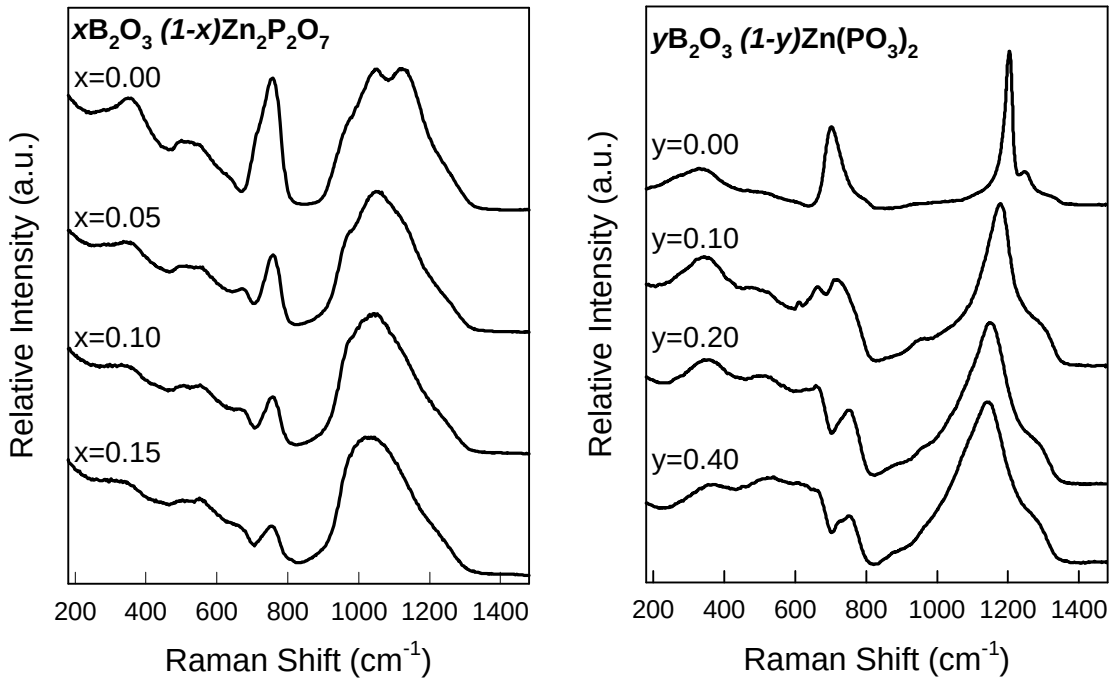

Figure 2-9: Raman spectra collected from several of the series I (left) and series II (right) glasses.

Table 2-6: Raman band assignments for the zinc borophosphate glasses.
Assignments are from Konijnendijk and Stevels (1975) and Brow *et al*. (1995).

Frequency (cm^{-1})	Series	Assignment
330-360	I,II	bend modes of phosphate polyhedra
500	I,II	bend mode related to Zn-phosphate network
512	II	bend mode related to B-phosphate network
555	I	diborate, or borate rings with multiple BO_4 groups
612	II	unidentified borate moiety
660-675	I,II	metaborate ring
702	II	POP symmetric stretch from metaphosphate tetrahedra
715-752	I	chain metaborates
757	I	POP symmetric stretch from pyrophosphate tetrahedra
969	I	PO_4 symmetric stretch (non-bridging oxygens)
1048	I	P-O-Zn stretch, Zn-phosphate network
1124	I	PO_3 symmetric stretch (non-bridging oxygens)
1143-1181	I,II	P-O symmetric stretch, B-phosphate network
1206	II	PO_2 symmetric stretch (non-bridging oxygens)
1250	II	PO_2 asymmetric stretch (non-bridging oxygens)
1310	II	P-O asymmetric stretch, B-phosphate network
1420-1450	I,II	nonbridging oxygen stretch, diborate

There are a number of changes in the Raman spectra when B_2O_3 is added to Zn-pyrophosphate. The peak at 1124 cm^{-1} is eliminated, the relative intensities of the peaks at 351 cm^{-1} and 757 cm^{-1} are reduced, and the intensity of the shoulder at 969 cm^{-1} increases with increasing B_2O_3 content. New bands, at 555 cm^{-1}, 673 cm^{-1}, and 1421 cm^{-1}, are present in the B_2O_3 containing glasses.

Figure 2-9 also shows the unpolarized Raman spectra collected from several of the series II glasses (right). The spectrum from the $Zn(PO_3)_3$ base glass is dominated by a narrow peak centered at 1206 cm^{-1} and a broader, asymmetric peak centered near 704 cm^{-1}. The former peak is due to the nonbridging $P\text{-}O^-$ symmetric stretch from Q^2 tetrahedra, and the latter is due to the bridging P-O-P symmetric stretch, also from neighboring metaphosphate tetrahedra (Brow *et al*. 1995). The lower intensity peak at 1250 cm^{-1} is due to the asymmetric PO_2 stretching mode, and the peak at 335 cm^{-1} is due to the bending modes of the phosphate tetrahedra. When B_2O_3 is added to this base glass, the high frequency peak broadens and shifts to lower wavenumbers, the 704 cm^{-1} gradually disappears, and new peaks, at 512, 663, 750, 950 cm^{-1}, and 1300 cm^{-1}, gradually appear.

Assignments to these new bands are given in Table 2-6. These assignments are mostly consistent with those made in Raman studies of a variety of other borophosphate compositions (Ray 1975; Scagliotti *et al*. 1987; Jin *et al*. 1989; Osaka *et al*. 1989; Sedmale *et al*. 1991; Ducel *et al*. 1993) and are discussed in detail below.

Oxygen bonding in zinc phosphate and zinc borophosphate (series II) glasses was also characterized by x-ray photoelectron spectroscopy; see Brow (1996) for additional details.

Figure 2-10 shows representative O*1s* spectra collected from the binary Zn-phosphate glasses. Each spectrum has a maximum centered near 532 eV and a lower intensity, higher energy shoulder centered near 534 eV. The relative intensity of the high binding energy contribution decreases with increasing ZnO-content. The inset to Figure 2-10 shows the results of curve-fitting into two Gaussian components for the O*1s* spectrum from the $50ZnO•50P_2O_5$ glass. Previous studies of simple phosphate glasses have related the high binding energy peak to bridging oxygens that link neighboring P-tetrahedra (P-O-P) and the low binding energy peak to nonbridging oxygens that are associated with a single P-tetrahedron ($P\text{-}O^-$) (Gresch *et al*. 1979; Onyiriuka, 1993); similar assignments are made for the two components in the spectra from these Zn-phosphate glasses.

Figure 2-11 shows the effect of composition on the quantitative oxygen bonding determined from the peak areas of each curve-fitted spectrum. Clearly, increasing the ZnO content depolymerizes the glass structure by replacing bridging P-O-P sites with nonbridging P-O-Zn sites. The dashed line in Fig. 2-11 is the predicted relationship between oxygen bonding and composition discussed below.

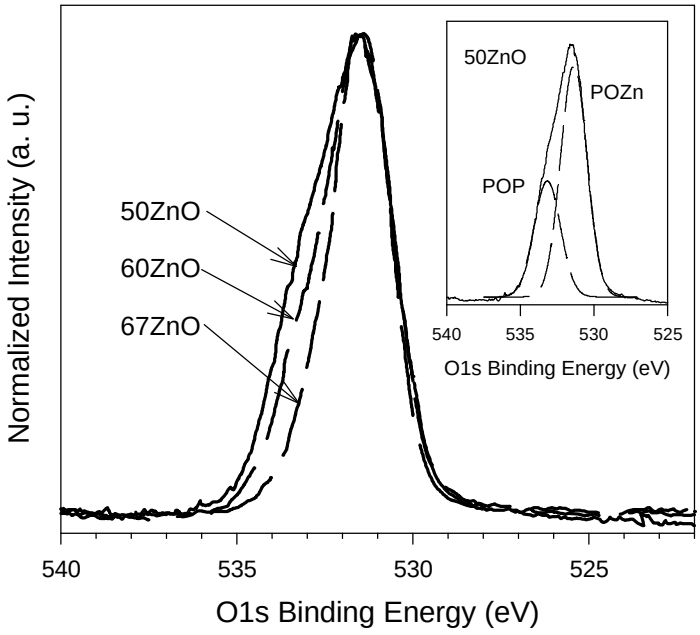

Figure 2-10: O1s spectra collected from several of the $xZnO•(1\text{-}x)P_2O_5$ glasses. The inset shows the decomposition of the $50ZnO•50P_2O_5$ spectrum into two Gaussian contributions.

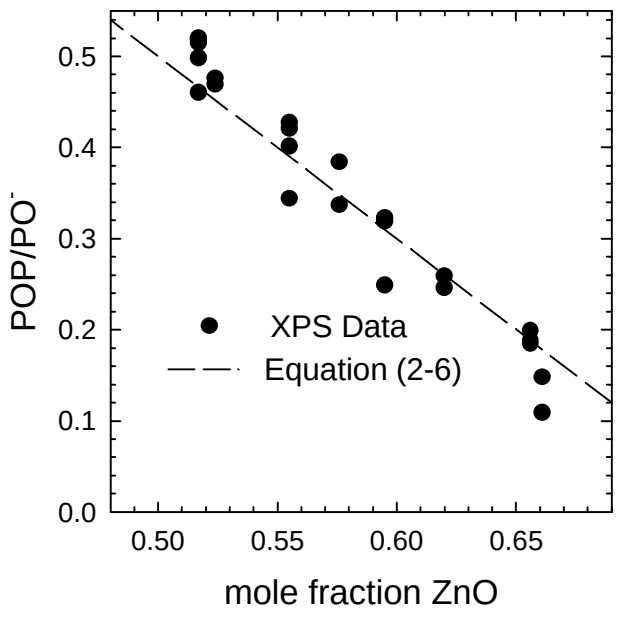

Figure 2-11: Quantitative oxygen bonding as determined from the decomposed O1s spectra of the xZnO•(1-x)P_2O_5 glasses. The dashed line is the expected relationship calculated from equation 2-6.

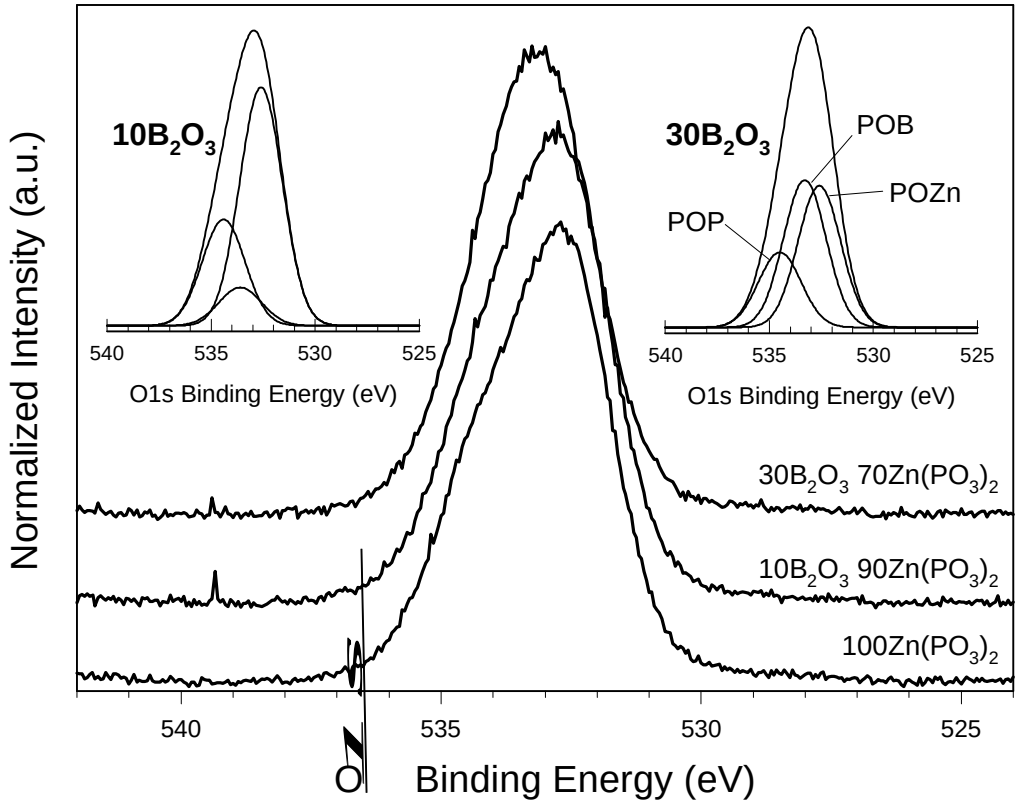

Figure 2-12: O1s spectra collected from several of the $yB_2O_3•(1-y)Zn(PO_3)_2$ glasses. The insets show the spectral decompositions with three Gaussian contributions.

Figure 2-12 shows some of the O*1s* spectra collected from the series II Zn-borophosphate glasses. In general, increasing the B_2O_3 content broadens the spectrum and shifts the peak to a slightly greater binding energy, from 532.6±0.3 eV in the $Zn(PO_3)_2$ glass to 533.2±0.3 eV in the $30B_2O_3•70Zn(PO_3)_2$ glass. These spectral changes can be understood by adding a third Gaussian component, with an intermediate binding energy, to the curve-fitting procedure (insets to Figure 2-12). This new feature, assigned to P-O-B sites, increases in intensity with increasing B_2O_3-content, relative to both the P-O-P and P-O-Zn sites. The intermediate binding energy of the P-O-B peak is consistent with the intermediate ionicity of this bond compared with the P-O-P and P-O-Zn bonds.

The effect of composition on the quantitative oxygen bonding in the borophosphate glasses is shown in Figure 2-13 (left). The relative intensities of both the POP and POZn contributions decrease and the POB peak intensity increases with increasing B_2O_3-content.

The depolymerizing effects of a divalent modifier (R') on the nature of a metaphosphate glass network can be summarized by the following reactions:

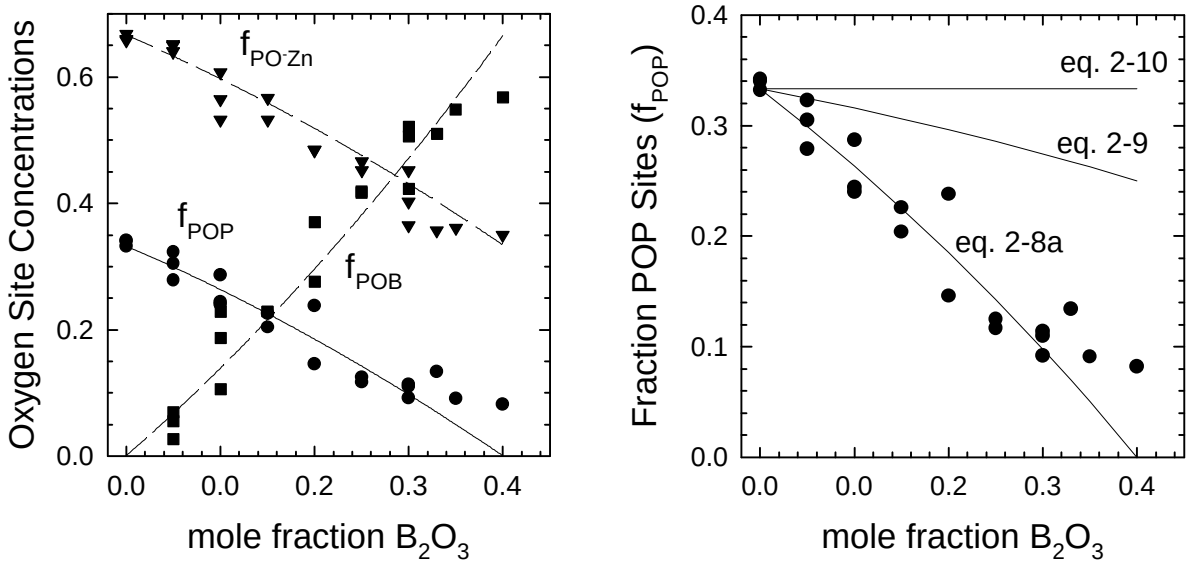

Figure 2-13: Quantitative oxygen bonding as determined from the decomposed O1s spectra of the yB_2O_3•$(1-y)Zn(PO_3)_2$ glasses (left). The dashed lines are the expected relationships calculated from equations 2-8(a-c). Predicted P-O-P relative intensities (right) based on the borophosphate model (eq. 2-8a), the phase separation model (eq. 2-9) and the metaborate model (eq. 2-10) discussed in the text; the filled symbols are from the decomposed O*1s* spectra

$$R'(PO_3)_2 + R'O \rightarrow R'_2P_2O_7 \qquad (2\text{-}5a)$$

$$2Q^2 + R'O \rightarrow 2Q^1. \qquad (2\text{-}5b)$$

The addition of the modifier depolymerizes the glass network by converting metaphosphate tetrahedra (Q^2, with two bridging oxygens and two nonbridging oxygens) to pyrophosphate tetrahedra (Q^1, with one bridging oxygen and three nonbridging oxygens). Gresch *et al*. (1979) showed that the quantitative oxygen bonding in such binary phosphate glasses is described by the relationship:

$$POP/PO^- = 0.5(3-4x). \qquad (2\text{-}6)$$

where x is the mole fraction of the modifying oxide (R'O). Equation 2-6 is plotted as the dashed line in Figure 2-11, where it is shown to closely agree with the quantitative oxygen bonding for the entire range of $xZnO•(1-x)P_2O_5$ glasses determined from the respective *O1s* spectral decompositions. XPS can thus provide an accurate description of the conversion of P-O-P bonds to P-O-Zn bonds with increasing ZnO-content. (Note that the oxygen bonding calculated from eq. 2-6 depends only on the Zn:P ratio; disproportionation of Q^1 sites in high [ZnO] glasses, as characterized by Raman and

NMR spectroscopies described above, does not affect the overall bridging-to-nonbridging oxygen ratio.)

Similar structural reaction models can be developed to explain the oxygen bonding trends for the Zn-borophosphate glasses. Such models will depend on the nature of the incorporated B-sites, which can be characterized by ^{11}B magic angle spinning nuclear magnetic resonance (MAS NMR). The ^{11}B MAS NMR spectra (Figure 2-8 above) from glasses with less than ~30 mole% B_2O_3 are dominated by a single, narrow peak centered at -3.8 ppm, due to BPO_4 groups (tetrahedral borons with P as the next nearest neighbor). Reaction (2-7) summarizes these spectroscopic trends:

$$2B_2O_3 + 3Zn(PO_3)_2 \rightarrow 4BPO_4 + Zn_3(PO_4)_2 \qquad (2\text{-}7)$$

This reaction presumes that bridging oxygen (P-O-P) associated with the metaphosphate base structure will be consumed to form the borophosphate bonds (P-O-B) and that the zinc ions, which no longer are required to neutralize the reacted Q^2 sites, will depolymerize others to form the orthophosphate (Q^0) species. For a $yB_2O_3 \bullet (1–y)Zn(PO_3)_2$ glass, the relative fractions of the three possible oxygen sites described by reaction (2-7) are:

$$f_{POP} = (2 - 5y)/(6 - 3y) \qquad (2\text{-}8a)$$
$$f_{POZn} = (4 - 6y)/(6 - 3y) \qquad (2\text{-}8b)$$
$$f_{POB} = 8y/(6 - 3y) \qquad (2\text{-}8c)$$

These relationships are expected to hold for y up to 0.40, at which point all $Zn(PO_3)_2$ has been consumed (reaction (2-7)) and the fraction of P-O-P sites (f_{POP}) goes to zero. (See Brow (1996) for how eqs. 2-8a-c are determined).

Figure 2-13 shows the oxygen bonding determined from the O*1s* spectra collected from the Zn-borophosphate glasses along with the predicted relationships based on eqs. 2-8(a-c). Reasonable agreement exists between the measured and predicted values up to ~30 mole% B_2O_3, the composition at which most borons are still incorporated into $B(OP)_4$ sites.

Figure 2-8 (right) reveals that a second narrow peak, centered at -1.8 ppm, and new, broad, asymmetric feature are present in the ^{11}B MAS NMR spectra from glasses with >30 mole% B_2O_3. These features are due to tetrahedral and trigonal B-sites, respectively, associated with separate zinc borate structures (as shown by the NMR results above and reported by Gan *et al*. (1994)). The resulting B-O-B and B-O-Zn bonds invalidate the 'three-oxygen' peak decomposition model used to analyze the O*1s* spectra from these B_2O_3-rich glasses. However, Figure 2-13 shows that XPS can provide useful, quantitative information about oxygen bonding in the simpler structures of ternary Zn-borophosphate glasses with up to ~30 mole% B_2O_3.

The predictions shown in Figure 2-13 are quite different from other possible interpretations of the O*1s* spectra, and so XPS can be used to distinguish between different quantitative structural models. Consider two alternate assignments for the intermediate binding energy peaks in the decomposed O*1s* spectra (Fig. 2-12) from the borophosphate glasses. First, if the addition of B_2O_3 to $Zn(PO_3)_2$ produced no new structures and the two components remained separate phases, the third O*1s* peak

might be due to B(3)-O-B(3) sites. If so, the fraction of bridging P-O-P sites for a $yB_2O_3 \bullet (1-y)Zn(PO_3)_2$ glass will depend on composition according to:

$$f_{POP} = (2 - 2y)/(6 - 3y). \qquad (2\text{-}9)$$

If, on the other hand, the B_2O_3 additions promoted additional phosphate cross-linking by scavenging the Zn-ions to form, for example, zinc metaborate structures (viz., $B_2O_3 + Zn(PO_3)_2 \rightarrow ZnB_2O_4 + P_2O_5$), the third O*1s* peak might be due to a combination of B-O-B and B-O-Zn sites. The fraction of P-O-P sites would then depend on composition according to:

$$f_{POP} = (2 - y)/(6 - 3y). \qquad (2\text{-}10)$$

The predictions of these latter models are compared with those of the borophosphate structural model (eq. 2-8a) in Figure 2-13 (right); the borophosphate model is clearly in better agreement with the XPS results than either the phase separation model (eq. 2-9) or the metaborate model (eq. 2-10). Other models can be similarly constructed and checked.

II-3 Tin Zinc Phosphate Glasses

Additions of Sn(II)O have been reported to stabilize the formation of Zn-pyrophosphate glasses to yield low melting temperature, chemically stable compositions for various sealing applications (Francis and Morena, 1994; Morena, 1996). We have examined several series of $SnO\text{-}ZnO\text{-}P_2O_5$ glasses, including compositions for which SnF_2 was substituted for SnO (Table 2-7).

Glasses were prepared from reagent grade ZnO, $NH_4H_2PO_4$, SnO, with nominal ZnO contents between 8.3 and 33.3 mole%. The analogues of these compositions were made substituting SnF_2 for SnO. Raw materials were thoroughly mixed, then melted in SiO_2 crucibles for 2 to 4 hours at temperatures ranging from 800°C to 1000°C. A variety of melt procedures were used in an effort to produce clear homogeneous glasses. N_2 was bubbled into some of the $SnO\text{-}ZnO\text{-}P_2O_5$ melts to reduce the likelihood of Sn(II)O oxidizing to $Sn(IV)O_2$. N_2 was also bubbled above the $SnF_2\text{-}ZnO\text{-}P_2O_5$ compositions to retain as much fluorine as possible. Whether or not N_2 was used appears to have had no appreciable affect on the appearance or measured properties of the glasses. Some batches were calcined at 230°C to slowly decompose the $NH_4H_2PO_4$ and others were charged into the crucible at elevated temperatures. Glasses were poured onto stainless steel plates and annealed at temperatures near T_g. Glasses made with SnF_2 generally required lower melting temperatures and fumed considerably, indicating substantial fluorine loss.

To varying degrees, most of the glasses contained white, unmelted material as well as bubbles. In the molten state most compositions consisted of two layers; a thin foamy or crusty skin covering or surrounding the clear fluid batch.

Glass transition (T_g) and crystallization temperatures (T_x) were determined by differential thermal analysis using heating rates of 20°C/min. Thermal expansion measurements were made using a fused

SiO_2 dual-rod dilatometer with an alumina reference. The chemical durability of the glass was determined from the measured weight loss of a sample suspended in de-ionized H_2O at 70°C. The rate of weight-loss (DR) is calculated from this measurement ($g/cm^2/min$). These properties are listed in Table 2-7.

In general, increasing the SnO:ZnO ratio decreases the glass transition temperature (T_g), increases the coefficient of thermal expansion (CTE), and increases the dissolution rate in de-ionized water. The most durable glasses are those with P_2O_5-contents at or below the pyrophosphate limit (33.3 mole%). Replacing SnO with SnF_2 slightly increases CTE and lowers T_g. It is unclear if these property changes are related to the incorporation of F into the glass structure. X-ray photoelectron spectroscopic analyses of the fracture surfaces of SnFZP-1 and SnFZP-3 failed to detect residual F.

Finally, a number of the glasses were used in Sessile drop experiments on float glass in air from temperatures ranging from 425°C to 500°C for 30 minutes to determine wetting and bonding behavior. The results of these experiments are summarized in Table 2-8.

Unpolarized and polarized Raman spectra were obtained with an excitation wavelength of 514 nm. Band assignments are similar to those made for the binary $ZnO-P_2O_5$ glasses (Table 2-3). In general, these analyses show that increasing the $[SnO+ZnO]/[P_2O_5]$ ratio causes the same phosphate network depolymerization noted for the series of binary $ZnO-P_2O_5$ glasses (*viz*., Figure 2-4). Changing the SnO/ZnO ratio, from 1:1 to 5:1 (Table 2-7) also produces variations in the Raman spectra, as shown in Figures 2-14 for 40 mole% P_2O_5, 2-15 for 33.3 mole% P_2O_5, and 2-16 for 30 mole% P_2O_5.

Changes in the respective peak frequencies most likely reflect the larger size (and so the lower field strength, defined as charge/(radius)^2) of Sn^{2+} compared with Zn^{2+}; Sn^{2+} has a crystal radius of 1.32Å compared with 0.88Å for Zn^{2+} (assuming both are octahedrally coordinated (Shannon (1976).) The lower field strength of Sn^{2+} will yield a smaller force constant for the bonds between the modifying cation and surrounding oxygens. In addition, the larger Sn^{2+} cation will likely increase the bond angle between nonbridging oxygens and P. Both trends are expected to decrease the frequency of the $(PO_2)_{sym}$ mode as SnO replaces ZnO (see, *e.g*., Rouse *et al*. 1978). This is most clearly evident in the series of glasses with 40 mole% P_2O_5 (Figure 2-14).

Narrowing of the $(PO_3)_{sym}$ band, centered near 1050 cm^{-1}, with increasing SnO, indicates that Sn^{2+} plays a different structural role than Zn^{2+} in the low P_2O_5 glasses (Figures 2-15 and 2-16). This band narrowing is accompanied by a decrease in the intensity of $(POP)_{sym}$ stretching band centered at ~745 cm^{-1} relative to the $(PO_3)_{sym}$ band, indicating a change in the polarizability of the P-nonbridging oxygen bonds. Again, the larger size of Sn^{2+} suggests more of a modifier role than Zn^{2+}, the latter of which assumes acts like a network cation (section II-1).

Table 2-7: Compositions and selected properties of tin- zinc phosphate glasses.

	Composition (mole%)										
glass name	**SnO**	**ZnO**	**P_2O_5**	**SnF_2**	**Na_2O**	**Li_2O**	**CTE (10^{-7}/°C)**	**T_g (°C)**	**T_x (°C)**	**DR**	**comments**
SnZnP-1	33.3	33.3	33.3				95	331	520	-5.8	mostly clear
SnZnP-2	44.4	22.2	33.3				105	323	579		mostly clear, melt 2,under N_2.
SnZnP-3	55.5	11.1	33.3				105	294	none		not clear, almost opaque.
SnZnP-4	35	35	30				92	336	503	-6.9	not very clear, full of floaters
SnZnP-4-md1	31	35	29		2.0	2.0		323	471		
SnZnP-5	30	30	40				111	314	808	-4.7	clear but quite a few bubbles
SnZnP-6	25	25	50				118	302	none	-3.1	somewhat clear, many bubbles.
SnZnP-7	46.7	23.3	30				110	315	504	-6.3	not very clear, full of floaters
SnZnP-8	40	20	40				120	299	none	-3.7	clear, a few bubbles, surf floaters.
SnZnP-9	33.3	16.7	50				133	278	none	-3.0	clear, full of bubbles.
SnZnP-10	58.3	11.7	30				122	291	462		mostly clear but many white floaters
SnZnP-11	50	10	40				145	269		-3.9	somewhat clear, floaters, bubbles.
SnZnP-12	41.7	8.3	50				146	264		-3.8	
SnFZP-1		33.3	33.3	33.3			94	332	500	-5.5	Glass mostly clear. N2 bubbling
SnFZP-2		22.2	33.3	44.4			110	308	682	-5.3	Glass clear but full of bubbles
SnFZP-3		11.1	33.3	55.5			132	273	none		Glass not very clear
SnFZP-4		35	30	35.0			99	323	490	-7.3	mostly clear
SnFZP-5		30	40	30.0			109	314	544	-3.7	clear glass with small bubbles
SnFZP-6		25	50	25.0							
SnFZP-7		23.3	30	46.7			109	303	435	-5.1	clear glass full of bubbles, white surf is layer of bubbles
SnFZP-8		20	40	40.0			122	282		-4.9	cloudy, translucent, many bubbles
SnFZP-9		16.7	50	33.0							cloudy, translucent, many bubbles
SnFZP-10		11.7	30	58.3			131	280	475		
SnFZP-11		10	40	50.0				272			mostly clear, some bubbles
SnFZP-12		8.3	50	41.7				253			cloudy, translucent. Some bubbles
											1st cook for short time, cleared up on remelt, Tg 268
SnZAP-1	53.3	11.7	30		2.5	2.5					
SnZAP-2	48.3	11.7	30		5.0	5.0	143	268	none		
SnZAP-3	43.3	11.7	30		7.5	7.5		261	434		

Table 2-8: Results of Sessile drop experiments with SnO-ZnO-P_2O_5 glasses

Glass Name	Temp/time	substrate	flow	Bond	xtals	Comments
SnZnP-1	475/1hr	float glass	yes	yes	yes	
SnZnP-2	500/30min	float glass	yes	no	????	
SnZnP-4	450/30min	float glass	no	no	none	
SnZnP-4	475/30min	float glass	yes	no	no	Slight flow (∠60°)
SnZnP-4mod1	425/30min	float glass				
SnZnP-5	500/30min	float glass	yes	no	yes	
SnZnP-7	475/30min	float glass	yes	no	maybe	good flow(∠30-45°)
SnZnP-8	500/30min	float glass	yes	no	no	flow (∠45°-50°)
SnZnP-10	425/30min	float glass	yes	no	none	
SnZnP-11	500/30min	float glass	yes	no	no	flow (∠60°)
SnFZP-1	425/30min	float glass	no	no	none	
SnFZP-1	475/30min	float glass	yes	yes	yes	
SnFZP-4	450/30min	float glass	no	no	none	
SnFZP-5	500/30min	float glass	yes	yes	yes	
SnFZP-7	400/30min	float glass	no	no	none	

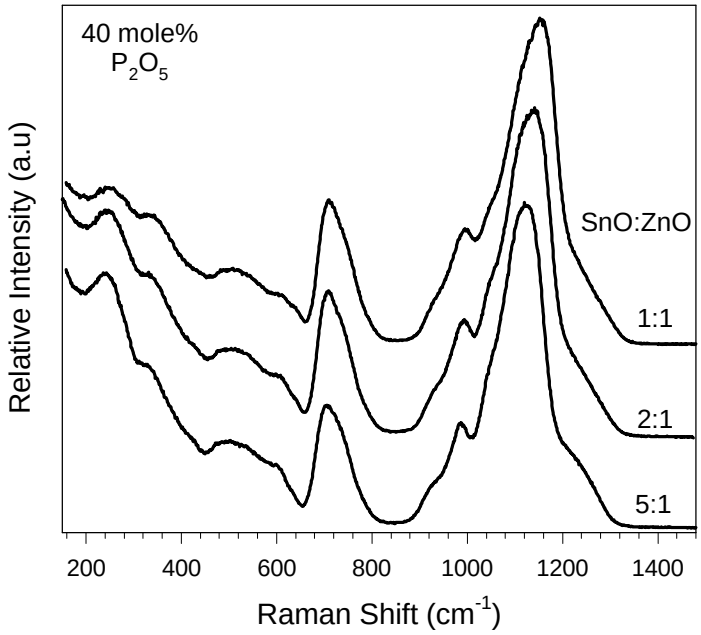

Figure 2-14: Raman spectra from glasses with 40.0 mole% P_2O_5 and different SnO:ZnO ratios.

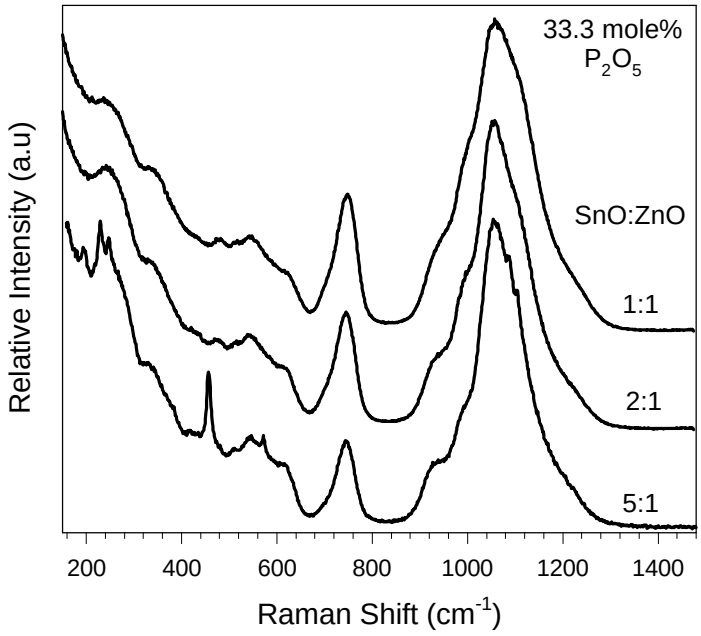

Figure 2-15: Raman spectra from glasses with 33.3 mole% P_2O_5 and different SnO:ZnO ratios.

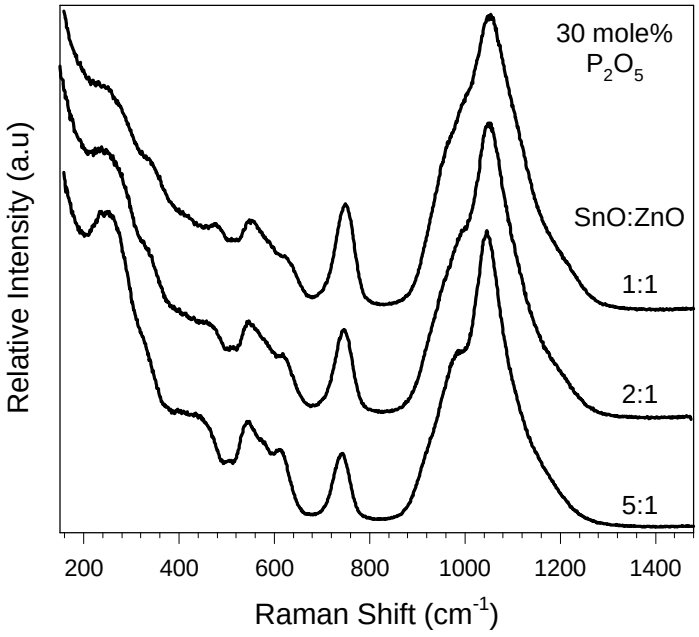

Figure 2-16: Raman spectra from glasses with 30.0 mole% P_2O_5 and different SnO:ZnO ratios.

The spectrum from the translucent sample of SnZnP-3 (55.5SnO 11.1ZnO 33.3P_2O_5) in Figure 2-15 shows evidence of a separate, crystalline phase. X-ray diffraction analysis of this sample showed it was primarily amorphous with a minor, unidentified, poorly-crystallized phase.

III. PbO-Free Sealing Glasses

III-1 Introduction

The information in this section is from the *Sandia Technical Advance SD- 5738*, dated Oct. 11, 1995.

PbO-based solder glasses are important materials for a variety of hermetic, low temperature, packaging applications. For example, they are used to seal float glass front and back panels for flat panel displays. A schematic of such a seal is shown in Figure 3-1. The requisite properties for the sealing glass include a close thermal expansion (CTE) match to the substrate and a sealing temperature low enough (generally <500°C) to avoid distorting the substrate and to be compatible with other components in the package.

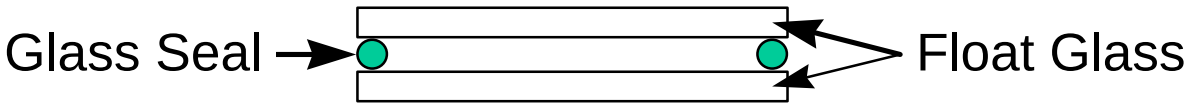

Figure 3-1: Schematic of a flat panel display seal.

There are a number of drawbacks associated with PbO-based solder glasses. The most serious is the toxicity of PbO which necessitates careful preparation and handling procedures and which makes components that contain PbO-based solder glasses candidates for regulatory action. In addition, PbO easily reduces to Pb-metal so that seals must be made in oxidizing atmospheres, a requirement that complicates their use in packages for air-sensitive components. Finally, the aqueous durabilities of PbO-solder glasses is relatively poor, thus making such-sealed packages susceptible to environmental corrosion.

Flat panel displays need to be evacuated (to $\approx 10^{-8}$ torr for field emitter displays and $\approx 10^{-3}$ torr for plasma displays) for proper operation. In order to achieve the required vacuum and then maintain it over long periods of continued operation, the glass panels which make up the display must be hermetically sealed. Current display technology requires that the sealing material be inorganic, electrically non-conductive, and able to maintain a hermeticity level of 1×10^{-8} atm cc/sec helium.

We describe below a new family of PbO-free glasses which have the requisite properties for many low temperature packaging applications, including hermetic flat panel displays. They have CTE-matches to float glass, they can be sealed at or below 500°C, they can be sealed in inert or

reducing atmospheres and they have aqueous durabilities superior to conventional PbO-based solder glasses. We have made seals to float glass both in furnaces and with a CO_2-laser.

III-2 Glass Compositions and Properties

These glasses are based on the Zn-phosphate glass-forming system (section II-1). Representative compositions are given in Table 3-1. (Appendix B contains the complete list of alkali-zinc phosphate glasses prepared and characterized in this study.) The compositions include mixed alkali oxides (typically less than 15 mole% total), alumina, boron oxide, and a transition metal oxide (e.g., Fe_2O_3, 2-4 mole%). These compositions are different from those recently patented by Corning, Inc. (Beall and Quinn 1990) in that they have more P_2O_5, less total alkali oxides, and generally less ZnO. Several representative Corning compositions are also given in Table 3-1. As a result, these new glasses have lower CTEs than the Corning glasses, making them candidates for specialized packaging applications. In addition, these new glasses contain transition metal oxides such as Fe_2O_3, which appear necessary for good bonding to float glass and which promote efficient absorption for laser sealing.

Glasses were prepared using standard melt processing techniques. Raw materials generally include alkali carbonates, Zn-, Al-, and Fe-oxides, boric acid, and $NH_4H_2PO_4$. Batches were mixed then melted in silica crucibles, usually around 1000-1200°C, for about an hour in air, then glasses were cast and annealed at the appropriate temperature.

Table 3-1: Compositions (mole%) of selected PbO-free, low temperature sealing glasses.

Glass	Li_2O	Na_2O	K_2O	ZnO	Al_2O_3	B_2O_3	Fe_2O_3	P_2O_5
ZFAP-2	3.0	3.0	3.0	39.7	3.0	4.3	2.0	42.0
ZFAP-3	3.0	5.0	3.0	39.7	4.0	3.3	3.0	39.0
ZFAP-9A	4.1	4.1	0.0	37.4	3.1	4.4	4.1	42.9
ZFP-30	5.0	5.0	0.0	42.0	6.0	4.0	2.0	36.0
ZFP-32	5.0	5.0	0.0	42.0	4.0	2.0	2.0	42.0
Corn. ZP1	6.0	7.0	7.0	43.0	2.0	0.0	($2.0SiO_2$)	33.0
Corn. ZP2	7.0	8.0	5.0	40.0	2.0	0.0	(5.0SnO)	33.0
Corn. ZP28	6.0	7.0	7.0	41.0	2.0	0.0	(4.0SnO)	33.0

Table 3-2: Selected properties of low temperature sealing glasses.

Glass	CTE (25-300°C)	T_g	T_{seal}	Diss. rate (g/cm^2-min)
ZFAP-2	94x10^{-7}/°C	406°C	550°C	2.5x10^{-6}
ZFAP-3	92x10^{-7}/°C	386°C	550°C	
ZFAP-9	90x10^{-7}/°C	394°C	550°C, laser	2.0x10^{-6}
ZPF-30	88x10^{-7}/°C	363°C	cryst.	
ZPF-32	98x10^{-7}/°C	342°C	500°C, laser	4.0x10^{-7}
SEM-COM SCB-2	91x10^{-7}/°C	351°C	480°C, laser	9.0x10^{-8}
SEM-COM SCC-1	109x10^{-7}/°C	309°C	430°C, laser	8.7x10^{-8}
Corning ZP-1	131x10^{-7}/°C	336°C	cryst.	
Corning ZP-2	121x10^{-7}/°C	332°C	cryst.	
Corning ZP-28	125x10^{-7}/°C	337°C	cryst.	7.5x10^{-9}

Table 3-2 lists some of the properties of these new glasses. Thermal expansion (CTE) was measured from 25°C to 300°C by dilatometry at 10°C/min. The glass transition temperature (T_g) was taken from the CTE curve. Aqueous durability was determined from weight loss measurements from bulk glass samples suspended in 70°C de-ionized water for three days. The PbO-based solder glasses listed in the Table were manufactured by SEM-COM Company (Toledo, OH) and are used to seal flat panel displays. The properties of the Corning Zn phosphate glasses from Table 3-1 are also given in Table 3-2.

In general, the new glasses have thermal properties that are comparable to those of the PbO-based solder glasses, although the new glasses do need higher temperatures to make a seal. The aqueous durability of the new glasses are comparable to the PbO-based solder glasses, but inferior to the Corning Zn-phosphate glasses. However, the new glasses have lower CTEs than the Corning composition, and so match the CTEs of substrates like float glass. In addition, the Corning glasses tend to crystallize when heated to sealing temperatures, whereas the new glasses flow and bond without significant crystallization.

III-3 Sealing Experiments

Seals were made by sandwiching pieces of the different sealing glasses between cleaned samples of float glass substrates (Figure 3-1) and then either heating the entire assembly in a furnace, either in air or in argon, to the sealing temperature and holding for about thirty minutes, or by locally heating the sealing glass using a CO_2 laser until it melted and bonded to the float glass.

Sealing temperatures noted in Table 3-2 are the lowest temperatures at which the respective glasses adhered to the float glass substrates. Fibers of ZPF-32 were drawn from melts and used as preforms for some of the float glass sandwich seals. The new glasses wet and strongly adhere to float glass at the temperatures indicated in Table 3-2. In general, their wetting behavior is inferior to the PbO-glasses, but superior to the Corning zinc phosphate glasses. Seals could be made with the new glasses, in each case listed in Table 3-2, without noticeable crystallization.

Sandia ZFAP-9 was provided in solid rod form and was sealed to float glass substrates in various furnaces where inert atmospheres were available. The absence of lead in the glass composition makes sealing in an inert atmosphere possible. Numerous sealing attempts eventually resulted in successful seals in a batch furnace, with Argon atmosphere and the following thermal cycle:

RT → 550°C @ 10°C/min, hold 10 min
550 → 390°C @ 10°C/min, hold 10 min
390 → RT @ 10°C/min

Coupon wetting samples with no top plate resulted in good flow and bonding, but the ZFAP-9 wetting angle with the substrate was greater than 90°, which would normally indicate a marginal affinity of the sealing glass for the substrate. However, sandwich seals with ZFAP-9 produced strong seals with better wetting angles of about 90°. The micrograph to the left (Figure 3-2) shows a typical cross-section of a ZFAP-9 sandwich seal made with the above process. The glass flowed and bonded well, and the wetting angle is about 90°. There were many small bubbles at the interface, but no cracking in either glass and no evidence of crystallization in the ZFAP-9.

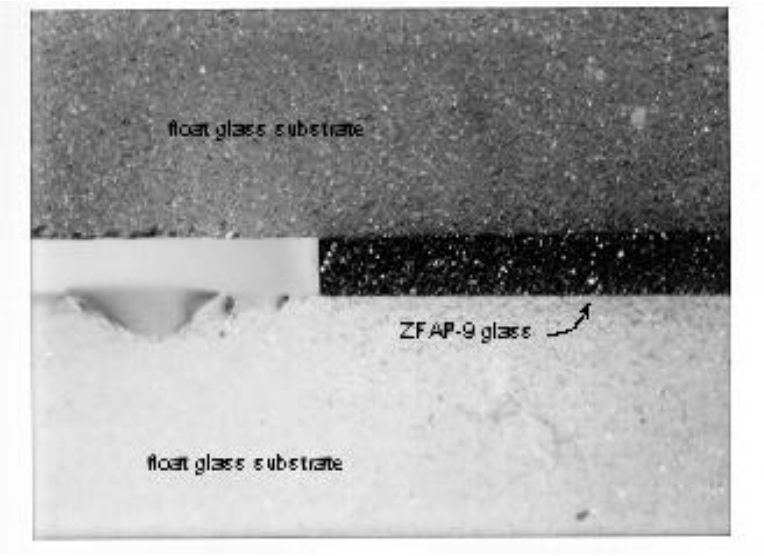

Figure 3-2: Optical micrograph of a sandwich seal between float glass and ZFAP-9.

Sealing temperatures below 550°C produced inadequate flow in the ZFAP-9 and consequently minimal bonding. The glass did not become fluid enough to create a good seal. Temperatures much above 550°C produced crystallization in the sealing glass and minor cracking in the float glass substrate.

The required sealing temperature of 550°C was too high for heated platen sealing of flat panel displays. ZFAP-9 may have applications in laser sealing of glass panels;, however, it was not used for laser sealing in this program, and no further sample sealing studies were conducted with it.

Sandia ZFP-32 was the second glass provided by the Sandia lead-free low temperature glass development program. It was a vitreous composition for sealing to float glass and was provided in solid rod form. Sandwich seals were made in various furnaces with inert Argon or Nitrogen atmospheres at temperatures up to 550°C. The glass did not exhibit sufficient flow at that temperature to produce a good seal. Given the schedule constraints and the lower temperature requirements for a sealing glass, sealing studies with ZFP-32 were concluded.

Summary and Conclusions

Highly depolymerized phosphate glasses, with structures based on pyrophosphate networks as indicated by various spectroscopic studies, are candidate materials for low temperature sealing applications. The short average chain length results in chemical durabilities that are lower than glasses based on metaphosphate structures. Thermal properties can be tailored by varying the type and concentration of modifying cations such that the resulting sealing glass is compatible with a variety of substrates. In addition, interesting glasses result when B_2O_3 is added as a second glass-forming oxide. The nature of the resulting borophosphate networks depends on the relative ratios of ZnO, B_2O_3, and P_2O_5, with desirable sealing glasses possessing a 'BPO_4' network.

Modified compositions are reported that have aqueous durabilities and thermal properties comparable to PbO-based solder glasses and that wet and bond to float glass when sealed both in a furnace and by a laser. Such glasses could be particularly useful for applications in which seals must be made in reducing atmospheres.

References

Y. Abe, 1983, in *Topics in Phosphorus Chemistry*, **Vol. 11**, ed. M. Grayson and E. J. Griffith, pp. 19-67, Wiley, New York

B. G. Aitken, D. C. Bookbinder, M. E. Greene, and R. M. Morena, 1993, "Non-Lead Sealing Glasses," US Patent 5,246,890, issued Sept. 21, 1993.

M. T. Averbuch-Pouchot, A. Durif, and M. Bagieu-Beucher, 1983, "Structure d'un Polyphosphate de Zinc, $Zn(PO_3)_2$," *Acta Cryst.*, Vol. C39, pp. 25-26.

G. H. Beall and C. J. Quinn, 1990, "Zinc-Containing Phosphate Glasses," US Patent 4,940,677, issued Jul. 10, 1990.

R. K. Brow, R. J. Kirkpatrick, and G. L. Turner, 1990, "The Short Range Structure of Sodium Phosphate Glasses. I. MAS NMR Studies," *J. Non-Cryst. Solids*, Vol. 116, pp. 39-45.

R. K. Brow, D. R. Tallant, S. T. Myers, and C. C. Phifer, 1995, "The Short Range Structure of Zinc Phosphate Glass," *J. Non-Cryst. Solids* Vol. 191, pp. 45-55.

R. K. Brow, 1996, "An XPS Study of Oxygen Bonding in Zinc Phosphate and Zinc Borophosphate Glasses," *J. Non-Cryst. Solids*, Vol. 194, pp. 267-273.

B. C. Bunker, D. R. Tallant, R. J. Kirkpatrick, and G. L. Turner, 1990, "Multinuclear magnetic resonance and Raman investigation of sodium borosilicate glass structures," *Phys. Chem. Glasses*, Vol. 31, pp. 30-41.

B. C. Bunker, R. J. Kirkpatrick, R. K. Brow, G. L. Turner, and C. Nelson, 1991b, "Local Structure of Alkaline-Earth Boroaluminate Crystals and Glasses: II, ^{11}B and ^{27}Al MAS NMR Spectroscopy of Alkaline-Earth Boroaluminate Glasses" *J. Amer. Ceram. Soc.*, Vol. 74[6], pp. 1430-38

C. Calvo, 1965, "The Crystal Structure of α-$Zn_3(PO_4)_2$," *Can. J. Chem.*, Vol. 43, pp. 436-445

J.F. Ducel, J.J. Videau, and M. Couzi, 1993, "Structural Study of Borophosphate Glasses by Raman and Infrared Spectroscopy," Phys. Chem. Glasses, Vol. 34, pp. 212-218.

G. L. Francis and R. Morena, 1994, "Non-Lead Sealing Glasses," US Patent 5,281,560, issued Jan. 25, 1994.

R. G. Frieser, 1975, A Review of Solder Glasses, *Electrocomponent Science and Technology*, vol. 2, pp. 163-199.

H. Gan, P. C. Hess, and R. J. Kirkpatrick, 1994, "Phosphorus and boron speciation in K_2O-B_2O_3-SiO_2-P_2O_5 glasses," *Geochim. Cosmochim. Acta*, Vol. 58[21], pp. 4633-47.

R. Gresch, W. Müller-Warmuth, and H. Dutz, 1979, "X-Ray Photoelectron Spectroscopy of Sodium Phosphate Glasses," *J. Non-Cryst. Solids*, Vol. 34, pp. 127-136

Jin Y, Chen X., and Huang X., 1989, "Raman Studies of Lithium Borophosphate Glasses," J. Non-Cryst. Solids, Vol. 112, pp. 147-150.

F. L. Knatak and F. A. Hummel, 1958, *J. Electrochem. Soc.*, Vol. 105[3], pp. 125

W. L. Konijnendijk and J. M. Stevels, 1975, *J. Non-Cryst. Solids*, Vol. 18, pp. 307-331.

E. Kordes, 1941, *Z. Phys. Chem.*, Vol. 50B, pp. 194

R. Morena, 1996, "Fusion Sealing Materials and Use in CRT," US Patent 5,514,629, issued May 7, 1996.

C. J. Quinn, G. H. Beall, and J. E. Dickinson, 1992, "Alkali Zinc Pyrophosphate Glasses for Polymer Blends," *Proceedings of the 16th Intenational Congress on Glass*, Vol. 4, pp. 79-84.

T. R. Meadowcraft and F. D. Richardson, 1965, "Structural and Thermodynamic Aspects of Phosphate Glasses," *Trans. Faraday Soc.*, Vol. 61, pp. 54-70.

E. C. Onyiriuka, 1993, "Zinc phosphate glass surfaces studied by XPS,", *J. Non-Cryst. Solids*, Vol. 163, pp. 268-273.

A. Osaka, M. Ikeda, K. Ezaki, Y. Miura, and K. Takahashi, 1989, "Network Structure of Borophosphate Glasses," *Nippon Seram. Kyokai Gak. Ronbunshi* Vol. 97[1]. pp. 274-78.

S. Prabhakar, K. J. Rao, and C. N. R. Rao, 1987, "A Magic-Angle Spinning P-31 NMR Investigation Of Crystalline And Glassy Inorganic Phosphates," *Chem. Phys. Lett.*, Vol. 139[1], pp. 96-102.

N.H. Ray, 1975, *Inorganic Polymers*, (Academic Press, London) pp. 79-90.

B. E. Robertson and C, Calvo, 1970, "Crystal Structure of α-$Zn_2P_2O_7$, *J. Solid State Chem.*, Vol. 1, pp. 120-133

G. B. Rouse, P. J. Miller, and W. M. Risen, Jr., 1978, "Mixed Alkali Glass Spectra and Structure," *J. Non-Cryst. Solids*, Vol. 28, pp. 193-207.

M. Scagliotti, M. Villa, and G. Chiodelli, 1987, "Short Range Order in the Network of the Borophosphate Glasses: Raman Results," *J. Non-Cryst. Solids*, Vol. 93, pp. 350-60.

G. Sedmale, J. Vaivads, U. Sedmalis, V. O. Kabanov, and O. V. Yanush, 1991, "Formation of Borophosphate Glass Structure within the System $BaO-B_2O_3-P_2O_5$," *J. Non-Cryst. Solids*, Vol. 129, pp. 284-291.

R. D. Shannon, 1976, "Revised Effective Ionic Radii and Systematic Studies of Interatomic Distances in Halides and Chalcogenides," *Acta Cryst*. Vol. A32, pp. 751-767.

G. L. Turner, K. A. Smith, R. J. Kirkpatrick, and E. Oldfield, 1986a, "Boron-11 Nuclear Magnetic Resonance Spectroscopic Study of Borate and Borosilicate Minerals and a Borosilicate Glass," *J. Magnet. Reson.*, Vol. 67, pp. 544-550.

G. L. Turner, K. A. Smith, R. J. Kirkpatrick, and E. Oldfield, 1986b, "Structure and Cation effects on phosphorus-31 NMR chemical shifts and chemical shift anisotropies of orthophosphate," *J. Magn. Resonan.*, Vol. 70**,** pp. 408-415.

J. R. Van Wazer, 1958, *Phosphorus and Its Compounds, Vol. 1*, Interscience Publishers, New York.

M. Villa, M. Scagliotti, and G. Chiodelli, 1987, "Short Range Order in the Network of the Borophosphate Glasses," *J. Non-Cryst. Solids*, Vol. 94, pp. 101-121.

W. A. Weyl and E. C. Marboe, 1964, *The Constitution of Glasses*, pp. 578-579, Interscience Publishers, New York.

Appendix A
Publications

1. R. K. Brow, D. R. Tallant, S. T. Myers, and C. C. Phifer, "The Short Range Structure of Zinc Phosphate Glass," *J. Non-Cryst. Solids* **191** 45-55 (1995) {SAND}

2. R. K. Brow, "An XPS Study of Oxygen Bonding in Zinc Phosphate and Zinc Borophosphate Glasses," *J. Non-Cryst. Solids*, **194** 267-273 (1996). {SAND94-0651J}.

3. R. K. Brow, L. Kovacic, and R. E. Loehman "Novel Glass Sealing Technologies," Proceedings of the International Symposium on Manufacturing Practices and Technologies, 1995 Fall Meeting Glass & Optical Materials Division, New Orleans, LA, Nov. 5-8, 1995. {SAND95-2866J}

4. R. K. Brow and Z. A. Osborne, "XPS Studies of Fluorine Bonding In Phosphate Glasses," *Surf. Interface Analyses*, **24** 91-94 (1996) {SAND95-1418J}

5. R. K. Brow and D. R. Tallant, "Structural Design of Sealing Glasses," Proceedings of the 14th University Congress on Glass Science, *J. Non-Cryst. Solids*, Lehigh University, June 18-20, 1997 {SAND97-0634J}.

Presentations

1. D. R. Tallant and R. K. Brow, "The Effect of Alkali, Zinc and Aluminum Ions on Phosphate Glass Structure," 96th Annual Meeting of the Amer. Ceram. Soc., Indianapolis, IN April 24-28, 1994. {SAND93-????A}.

2. R. K. Brow, "X-Ray Photoelectron Spectroscopic Studies of Glass 'Structure': Artifacts and Opportunities," (INVITED) 97th Annual Meeting of the Amer. Ceram. Soc., Cincinnati, OH April 30-May 4, 1995. {SAND94-3035A}.

3. R. K. Brow and L. Kovacic, "Novel Glass Sealing Technologies," 1995 Fall Meeting Glass & Optical Materials Division, New Orleans, LA, Nov. 5-8, 1995 {SAND95-1394A}.

4. R. K. Brow, D. N. Bencoe, and L. Kovacic, "PbO-Free Glasses For Low Temperature Hermetic Packages", 7th Annual Joint Meeting of the New Mexico Sections of the American Ceramic Society and the Materials Research Society, Albuquerque, NM, Oct. 30, 1995 {SAND95-2032A}

Patents/Technical Advances

1. R. K. Brow, "PbO-free sealing glasses for low temperature hermetic packages," **S-85,018, SD-5738** (Disclosure made Oct. 11, 1995).

Appendix B: Composition and properties of alkali zinc phosphate glasses

glass name	composition (mole%) ZnO	P_2O_5	Na_2O	Li_2O	Al_2O_3	B_2O_3	K_2O	BaO	SnO SiO_2	MoO_3 Fe_2O_3	WO_3 Cu_2O	CuO	25-300 CTE(10-7/C)	°C T_g	°C T_x	log DR g/cm^2min	comments
ZAP-1	44	33	10	10	3								125	345	~475		
ZAP-2	44	33	5	5	3			10					104	405	546		
ZAP-3	56.7	33.3	10										96(TMA)	375	~480		
ZAP-4	46.7	33.3	20										132(TMA)	~340	?525		swirls-phase sep?
ZAP-5	33.3	33.3	33.3										133(TMA)	312	460		some surf. xtals
ZAP-6	66.7	33.3											76	450	535		
ZAP-7	51.7	33.3	5	5		5							84(TMA)	380	525		
ZAP-8	49	33	6	6	3	3								375	515		milky
ZAP-9	42.7	42	4	4	3	4.3							88	381	587		
ZAP-9A	40.7	42	4	4	3	4.3	2							381			
ZAP-9A	40.7	42	4	4	3	4.3	2						97			-5.3	
ZAP-10	8	33	5		21	9	24						138	439	566		swirls & white floaters,melt#3
ZAP-11	8	25.5	5		30.5	9	23										glassy but white swirls
ZAP-12	50	25	12.5	12.5													did not make a glass
CuZAP-1,	41.7	40	3	3	3	4.3	3		2								
CornZP-1,	43	33	7	6	2		7		2				136	331	485		xtals or floaters in glass
CornZP-2	40	33	8	7	2		5		5								full of clear floaters, cloudy
CornZP-2	40	33	8	7	2		5		5							-8.3	glass is white
CornZP-28	41	33	7	6	2		7		4				131	338	499?	-8.6	
ZFAP-2																-5.6	
ZFAP-3	39.7	39	3	5	4	3.3	3			3			92	404	629		portion melted at 1250C
ZFAP-9A																-5.7	
ZPF-28	41	33	7	6	2		7			4			137	354	490?	-8.7	
ZPF-29	41	35	5	5	5	4	3			2			100	393	569?		
ZPF-30	42	36	5	5	6	4				2			88	401	478		

glass name	ZnO	P_2O_5	Na_2O	Li_2O	Al_2O_3	B_2O_3	K_2O	BaO	SiO_2	Fe_2O_3	Cu_2O	CTE(10-7/C)	T_g	T_x	log DR	
ZPF-33	42	42	4	4	4		2			2		111	367	564		
ZPF-34	44	33	5	5	11					2						did not make a glass @ 1300C in SiO2
ZPF-35	42	40	3	7	5					3		96	380	525		
ZPF-36	42	39	5	3	5		4			2		109	375	533		
ZPF-37	42	38	6	6	4	2				2		101	371	525	-6.4	
ZPF-38	42	35	4	6	4	2			3		4	101	364	484		green glass, not homogenous
ZPF-39	42	40	5	5	4	2				1	1	104	362	557	-5.5	dark purple glass

Distribution

Unclassified, Unlimited Release

1	MS	9018	Central Technical Files, 8940-2
5		0899	Technical Library, 4916
2		0619	Review & Approval Desk, 12690 For DOE/OSTI
1	MS	0188	LDRD Office, 4523
5	MS	1349	R. K. Brow, 1833
1		1411	D. R. Tallant, 1824
1		1349	D. N. Bencoe, 1833
1		0873	L. Kovacic, 14403
1		0367	B. K. Damkroger, 1833
1		1411	J. M. Phillips, 1824